FABRICATION OF POLYMERIC NANO-COATINGS VIA CHEMICAL VAPOR DEPOSITION

A Thesis Submitted to
The Graduate School of Engineering and Sciences of
Izmir Institute of Technology
In Partial Fulfillment of the Requirements for the Degree of

MASTER OF SCIENCE

in Chemical Engineering

by
Sema KIRKÖSE

December 2016
İZMİR

We approve the thesis of **Sema KIRKÖSE**

Examining Committee Members:

_____

Assist. Prof. Dr. Özgenç EBİL
Department of Chemical Engineering, Izmir Institute of Technology

_____

Assist. Prof. Dr. Güler NARİN
Department of Chemical Engineering, Uşak University

_____

Assist. Prof. Dr. Ayben TOP
Department of Chemical Engineering, Izmir Institute of Technology

27 December 2016

_____

Assist. Prof. Dr. Özgenç EBİL
Supervisor, Department of Chemical Engineering, Izmir Institute of Technology

_____

Prof. Dr. Fehime Seher ÖZKAN
Head of the Department of Chemical Engineering

_____

Prof. Dr. Bilge KARAÇALI
Dean of the Graduate School of Engineering and Sciences

ACKNOWLEGEMENTS

I would like to express my sincere gratitude to my supervisor Assist. Prof. Dr. Özgenç EBİL whose knowledge, understanding, patience, guidance, valuable advice and also encouragement added considerably to my graduate experience and helped me complete my M.Sc. thesis. I have benefited greatly from his direction and valuable comments during this study.

I would like to thank the Center for Materials Research (İYTE-MAM) staff, Center for Environmental R&D staff and Dr. Hüseyin ÖZGENER for their help with SEM and FTIR analyses. I would like to thank Aysel TOMAK for her help with AFM analysis. I wish to thank the whole staff of Department of Chemical Engineering for their help and technical assistance.

I would also like to thank my friends; Merve ÖZPİRİN, Gizem PAYER, Selcan ATEŞ for their help in laboratory work and friendship. I would like to present my deepest thanks to my friends; Selen EKİNCİ, Esin IŞIK, Cengizhan PAŞAOĞLU and Aybike Nil OLCAY for their friendship. My special thanks to Ali BEYAZNAR for his grateful advices, endless help, devotion, understanding, and support at the beginning and during my master thesis.

This journey would not have been possible without the support of my family. I am very grateful to my parents for their devotion, understanding, and support throughout my life. They always encouraged me in my graduate endeavor.

ABSTRACT

FABRICATION OF POLYMERIC NANO-COATINGS VIA CHEMICAL VAPOR DEPOSITION

Thin film coatings are used to provide protection to the substrate of interest against physical and chemical elements. Coating can also be applied to modify the surface properties of the substrate. One of the most important aspects of coating processes is controlling the thickness of coating material over the substrate. As a subset of a family of chemical vapor deposition methods, iCVD relies on vapor-to-surface reactions to form solid ultrathin polymer films. Unlike other CVD methods, iCVD is unique in that a polymerization reaction is induced by a thermally or chemically activated initiator molecule, much like in liquid-based thermal polymerization except without the use of a liquid solvent medium.

The aim of the study is to fabricate polymeric protective nano-coatings via iCVD on flat surfaces at low or ambient temperatures. A variety of polymers, including homopolymers of glycidyl methacrylate (GMA), cyclo hexyl methacrylate (CHMA) and 1H, 1H, 2H, 2H,-Perfluorodecyl acrylate (PFDA) and P(GMA-PFDA) copolymers were fabricated via iCVD. The surface roughness and contact angle values were measured. Smooth hydrophobic surfaces having high contact angle (approximately 130˚) were obtained with PPFDA and PGMA-co-PPFDA thin films. Chemical compositions of the homo and co-polymer films were also evaluated confirming the retention of functional groups during polymerization, thus opening possibility of using iCVD produced films in various sensor applications.

ÖZET

POLİMERİK NANO KAPLAMALARIN KİMYASAL BUHAR BİRİKTİRME YOLUYLA ÜRETİMİ

Koruyucu ince film kaplamalar alttaşların fiziksel ve kimyasal elementlere karşı korumasını sağlamak için kullanılır. Kaplama alttaşın yüzey özelliklerini değiştirmek için de uygulanabilir. Kaplama proseslerinin en önemli noktalarından biri alttaş üzerindeki kaplama kalınlığının kontrol edilmesidir. Kimyasal buhar biriktirme (KBB) yöntemlerinden biri olan iCVD, çok ince polimer filmler oluşturmak için buhardan-yüzeye olan reaksiyonlara dayanır. Diğer KBB metotlarından farklı olarak, iCVD ısı veya kimyasal reaksiyonlarla aktive edilmiş başlatıcı moleküllerin katı yüzey üzerinde polimerizasyon reaksiyonunu başlattğı, herhangi bir çözgenin kullanılmadığı bir KBB metodudur.

Bu çalışmanın amacı polimerik koruyucu nano kaplamaları iCVD yöntemi ile düz alttaşlar üzerinde, ortam sıcaklığına üretmektir. Glisidil metkrilat (GMA), sikloheksil metakrilat (CHMA) ve 1H,1H,2H,2H,-Perfloro desil akrilat (PFDA) homopolimerleri ve GMA-PFDA kopolimerleri içeren polimer filmer iCVD vasıtasıyla üretildi. Yüzey pürüzlülüğü ve temas açısı değerleri ölçüldü. Yüksek temas açısına sahip (yaklaşık 130˚) pürüzsüz hidrofobik yüzeyler PPFDA ve PGMA-PPFDA ince filmleri ile elde edildi. Çeşitli sensör uygulamalarında iCVD ile üretilen filmlerin kullanılabilirlik imkanından dolayı homo ve kopolimer filmlerin kimyasal komposizyonları polimerizasyon esnasında fonksiyonel grupların korunmasını doğrulayarak değerlendirildi.

TABLE OF CONTENTS

LIST OF FIGURES viii

LIST OF TABLES x

CHAPTER 1. INTRODUCTION 1

1.1. Materials and Their Varieties 1

1.1.1. Metals 1

1.1.2. Ceramics 2

1.1.3. Polymers 2

1.1.4. Composites 3

1.2. Coatings 4

1.3. Optical Coating Theory 6

1.4. Optical Coating Materials and Processes 11

1.4.1. Optical Coating Materials 12

1.4.2. Optical Coating Production Processes 18

1.5. Initiated Chemical Vapor Deposition (iCVD) Process 31

CHAPTER 2. EXPERIMENTAL WORK 39

2.1. Materials 39

2.1.1. Cleaning Procedures for Substrates 40

2.2. CVD Experimental Set-Up 42

2.3. Thin Film Deposition 44

2.4. Characterization 47

CHAPTER 3. RESULTS AND DISCUSSION 48

3.1. Fabrication of PGMA, PCHMA, PPFDA and P(GMA-PFDA) Thin Films 48

3.2. SEM Analysis of Thin Films 49

3.2.1. SEM Analysis of PGMA Thin Films 49

3.2.2. SEM Analysis of PCHMA Thin Films 52

3.2.3. SEM Analysis of PPFDA Thin Films 53

3.2.4. SEM Analysis of P(GMA-PFDA) Thin Films 55
3.3. FTIR Analysis of Monomers and Thin Films 56
3.3.1. FTIR Analysis of GMA Monomer and PGMA Thin Films 57
3.3.2. FTIR Analysis of CHMA Monomer and PCHMA Thin Films ... 58
3.3.3. FTIR Analysis of PFDA Monomer and PPFDA Thin Films 59
3.3.4. FTIR Analysis of P(GMA-PFDA) Thin Films 60
3.4. AFM Analysis of Thin Films 62
3.4.1. AFM Analysis of PGMA Thin Films 62
3.4.2. AFM Analysis of PCHMA Thin Films 64
3.4.3. AFM Analysis of PPFDA Thin Films 64
3.4.4. AFM Analysis of P(GMA-PFDA) Thin Films 65
3.5. Contact Angle Measurement of Thin Films 66
3.6. Performance Tests for Homopolymer and Copolymer Films 71

CHAPTER 4. CONCLUSIONS 73

REFERENCES 75

APPENDIX A. CALIBRATION GRAPHS 82

LIST OF FIGURES

Figure **Page**

Figure 1.1. The applications of the plating method 5
Figure 1.2. Anti-scratch coating 6
Figure 1.3. Electromagnetic spectrum 7
Figure 1.4. The light rays behaviors 9
Figure 1.5. Illustration of incident, refracted rays and their angles 9
Figure 1.6. a) Field vectors of the incident, transmitted, and reflected waves in case the electric field vectors lie within the plane of incidence (P polarization). (b) Field vectors of the incident, transmitted, and reflected waves in case the electric field ve ctors are perpendicular to the plane of incidence (S polarization) 10
Figure 1.7. Schematic diagram of thermal evaporation system. 19
Figure 1 8. Schematic diagram of electron beam evaporation system. 21
Figure 1.9. Schematic diagram of sputtering deposition system. 22
Figure 1.10. Schematic diagram of metal-organic chemical vapor deposition (MOCVD) system. 24
Figure 1.11. Schematic diagram of atomic layer deposition (ALD) 25
Figure 1.12. Schematic diagram of hot-wire chemical vapor deposition 26
Figure 1.13. Schematic diagram of plasma enhanced chemical vapor deposition (PECVD) system. 27
Figure 1.14. Schematic diagram of photo-initiated chemical vapor deposition (PICVD) system. 27
Figure 1.15. Stages of the dip coating process: (a) dipping of the substrate into the coating solution, (b) wet layer formation by withdrawing the substrate, (c) the thin film layer deposition by drainage, (d) the solvent evaporation by curing 29
Figure 1.16. Schematic diagram of the spin coating process: dripping solution on the surface, spin up, spin off and thin film formation by solvent evaporation. . 30
Figure 1.17. Reaction mechanism proposed for iCVD polymerization 31
Figure 1.18. A photo (a) and a schematic (b) representation of the iCVD reactor setup for coating on the surface of the substrate 32

Figure 2.1. The cleaning procedure for glasses 41
Figure 2.2. The RCA cleaning procedure for silicon wafer..... 42
Figure 2.3. CVD reactor geometry 43
Figure 2.4. The SemiconSoft, Inc. measurement instrument..... 47
Figure 3.1. SEM images of PGMA thin film on c-Si substrate..... 50
Figure 3.2. SEM images of the cross sectional areas of PGMA thin film on c-Si 50
Figure 3.3. SEM image of the surface of uncoated c-Si substrate..... 51
Figure 3.4. SEM image of the surface of ~1μm PGMA thin film on c-Si 51
Figure 3.5. SEM image of the PCHMA thin film on c-Si 52
Figure 3.6. SEM image of the edge of PCHMA thin film on c-Si 52
Figure 3.7. SEM image of the surface of PPFDA thin film on c-Si..... 53
Figure 3.8. SEM image of the cross section of PPFDA thin film on c-Si..... 53
Figure 3.9. SEM image of the surface of uncoated tissue paper 54
Figure 3.10. SEM image of the surface of PPFDA thin film coated on tissue paper 54
Figure 3.11. SEM image of the surface of ~1000 nm copolymer thin film on c-Si 55
Figure 3.12. SEM image of the cross sectional area of 656 nm copolymer thin film on c-Si 55
Figure 3.13. SEM image of the cross sectional area of ~1000 nm copolymer thin film on c-Si..... 56
Figure 3.14. FTIR spectra of monomer and polymer form of GMA thin film on c-Si .. 57
Figure 3.15. FTIR spectra of monomer and polymer form of CHMA thin film on c-Si 58
Figure 3.16. FTIR spectra of monomer and polymer form of PFDA thin film on c-Si . 59
Figure 3.17. FTIR spectra of ~1000 nm thick P(GMA-PFDA) thin film on c-Si 60
Figure 3.18. FTIR spectra of ~656 nm thick P(GMA-PFDA) thin film on c-Si 61
Figure 3.19. AFM results of uncoated c-Si substrate (a) color map (b) 3D view..... 62
Figure 3.20. AFM results of 1430 nm PGMA thin film on c-Si (a) color map (b) 3D view..... 63
Figure 3.21. AFM results of 367 nm PGMA thin film on c-Si (a) color map (b) 3D view..... 63
Figure 3.22. AFM results of 975 nm PCHMA thin film on c-Si (a) color map (b) 3D view..... 64
Figure 3.23. AFM results of 390 nm PPFDA thin film on c-Si (a) color map (b) 3D view..... 64

Figure 3.24. AFM results of 1000 nm thick P(GMA-PFDA) thin film on c-Si (a) color map (b) 3D view 65
Figure 3.25. AFM results of 656 nm thick P(GMA-PFDA) thin film on c-Si (a) color map (b) 3D view 66
Figure 3.26. The contact angle measurement of the uncoated c-Si 67
Figure 3.27. The contact angle measurement of the PPFDA thin film coated on c-Si... 67
Figure 3.28. (a) The uncoated c-Si and (b) PPFDA thin film coated on c-Si..... 68
Figure 3.29. PPFDA thin film coated paper 68
Figure 3.30. (a) PPFDA thin film coated tissue paper and (b) the uncoated tissue paper 68
Figure 3.31. The contact angle measurement of the PPFDA thin film coated tissue paper..... 69
Figure 3. 32. The contact angle measurement of ~ 1000 nm P(GMA-PFDA) thin film on c-Si 69
Figure 3.33. The contact angle measurement of 656 nm P(GMA-PFDA) thin film on c-Si 70
Figure 3.34. The contact angle measurement of ~500 nm PGMA thin film on c-Si..... 70

LIST OF TABLES

Table **Page**

Table 2.1. Properties of materials used in cleaning process and experiment 40

Table 2.2. The experimental parameters for thin film deposition 46

Table 3.1. The results of thin film deposition experiments 48

CHAPTER 1

INTRODUCTION

1.1. Materials and Their Varieties

There are many different ways to classify materials. Materials are basically divided into three groups such as metals, ceramics and polymers. This classification is based on materials properties such as chemical, physical, electrical, magnetic and optical etc. In addition to these materials, composites are one of the material groups, they are formed by combination of two or more materials like metals, ceramics and polymers (Callister, 2010; Askeland et al., 2010). These material types, their characteristics and applications are explained briefly in the next parts.

1.1.1. Metals

Metals contain one or more metallic elements like nickel, titanium, gold, iron and aluminum so on, and nonmetallic elements such as carbon, nitrogen and oxygen .When the structure of metals are considered, they are described as solid elements which are denser than the other elemental substances which are ceramics, polymers and composites (Callister, 2010). They have many features such as hardness, elasticity, resilience, ductility, and malleability. They are defined as good conductors because they transmit electricity and heat. At the same time, they have a high light reflection capacity.

Metals are used in many different application areas by taking into consideration their beneficial properties. These application areas are computers, transportation especially cars, buses, and trucks etc., prostheses used in biomedical, aerospace, electrical power production and distribution, farming and also household conveniences such as ovens, dish and clothes washers etc. (Lewis, 2015).

1.1.2. Ceramics

Ceramics are inorganic non-metallic compounds composed of metallic and nonmetallic elements such as oxides, carbides and nitrides that have been shaped and hardened by heating to high temperatures. Ceramics can be divided into two classes: traditional and advanced. Advanced ceramics include aluminum oxide or alumina (Al_2O_3), silicon dioxide (or silica, SiO_2), silicon carbide (SiC), silicon nitride (Si_3N_4) boron carbide (B_4C), and molybdenum disilicide ($MoSi_2$), while traditional ceramics consist of clay products, silicate glass and cement (Callister, 2010; Lewis, 2015).

There are two chemical bonds which keep together the atoms in ceramic materials; covalent and ionic. However, the atoms in metals have another type of chemical bond which is called metallic bond that weaker than covalent and ionic bonds. Therefore, when the ceramic materials and metals are compared, ceramic materials are brittle and extremely sensitive to fracture, however, metals are ductile. Besides, ceramic materials have low electricity due to the atomic structures and are more resistant to corrosion, high temperatures and also severe environmental effects than the other material types such as metals and polymers. They can be transparent, translucent or opaque (Callister, 2010; web1).

Due to a wide range of properties, ceramic materials are used in many different applications. For instance, these are high temperature glass windows, thermal barriers, fuel cells products in aerospace, glassware, windows, pottery, magnets, lenses, microwave transducers in consumer uses, ceramic filters, vibration sensors, oxygen sensors, safety glass windshields, in automotive, fiber optic/laser communications, TV and radio components in communications where ceramics are used (Lewis, 2015).

1.1.3. Polymers

Polymers are defined as organic materials because most of them are made of organic compounds, which are called as monomers, and generally they are based on hydrogen, carbon, and also nonmetallic elements such as oxygen, nitrogen and silicon (Askeland & Fulay et al., 2010). Moreover, these monomer molecules are bonded together in long repeating chains. As a result of this chemical process called as polymerization (web2), there are many polymers are formed which are very familiar such

as polyethylene (PE), polypropylene (PP), polystyrene (PS), polyethylene terephthalate (PET), and silicone rubber so on. (Callister, 2010). The densities of polymers are lower than the metals and ceramics, so the mechanical properties of polymers are not similar to other materials. Polymers are generally not stiff or strong, and also they are light in weight with changing degrees of strength. Polymers have lower densities and strength (Şen, 2015). Based on physical properties, polymers can be classified as thermoplastic, thermoset and elastomer. At room temperature, thermoplastic polymers are rigid. However, when thermoplastic polymers are heated, they can become soft and be reshaped (Roberts & Caserio, 1977). Moreover, they have good ductility (Askeland & Fulay et al., 2010). At room temperature or above thermosetting polymers can be shaped, but when they are heated, they can become stronger, infusible and brittle because the molecular chains are connected firmly. Elastomers are elastic materials such as rubbers and rubberlike (Roberts & Caserio, 1977). Furthermore, polymers can be quite good resistant to chemical, thermal and also electrical insulators, so they have a wide range of application areas such as medicine, industry, science, adhesives, coatings, packaging materials, textile, industrial fibers, composites, and also optical devices so on (Lewis, 2015, Askeland & Fulay et al., 2010).

1.1.4. Composites

Composites are defined that the two or more different materials such as metals, ceramics and polymers are combined together to improve their properties, to create excellent and unique materials by associating with the best characteristics of each of the component materials. Composite materials include metal composites, ceramic composites (composite ceramic and metal matrices), and composite building materials, such as cements, concrete, fiberglass which is made by spreading glass fibers in a polymer (web3). The glass fibers which are stiff and strong but brittle, make the polymer stiffer. By using composite materials, ductile, strong, lightweight and, temperature-resistant materials are produced (Askeland & Fulay et al., 2010). In addition, recently reinforced plastics such as fiber-reinforced polymer and carbon fiber-reinforced polymer are used as composite materials in advanced aircraft and aerospace vehicles (Callister, 2010). At the same time, composites are used in the production of sports equipment such as bicycles,

tennis rackets, golf clubs and especially F1 racing cars bodies to make lightweight, stiff and durable (web4).

Additionally, all materials and their applications mentioned above, nowadays, coating is one of the most used applications for different fields. The coating provides some useful properties to these materials taking advantage of their characteristic features. The coating will be explained in the next section in detail.

1.2. Coatings

Coatings are thin or thick layers that are applied to the surface of an object which is called 'substrate'. The role of a coating is to provide abrasion, scratch, fire, and heat and corrosion resistance. The coating may be applied to improve physical appearance and aesthetics decoratively and also for sealing ability and changing wettability. Another goal of the coating is to gain resistance against general wear, erosion, pitting, cavitation and also release or nonstick property (web5).

For decoration, paints and lacquers are coating to protect the substrate and also to prevent corrosion the paint is used for industrial pipes. Functional coatings can be applied to modify the surface properties or to gain new features to the surface. In recent years, cooking pans which are made from PTFE (polytetrafluoroethylene) coated on the surfaces of the metal pans have been used for non- stick surfaces. Moreover, ceramics, enameled cast iron and also silicon are used for similar applications and changing surface properties (web6; web7)

One of the functional coatings is catalytic coating which is formed by thermal-chemical deposition method. The method requires thermal, adhesion and catalytic properties for metal supports. Metal supports can be chosen as titanium, nickel, aluminum etc. (Babilius & Babilius et al., 2014). Self-cleaning glass can be given as an example of catalytic surface. They are used in sanitary facilities. Easy to clean surfaces are desirable, so titanium dioxide can be coated to provide self-cleaning and elimination of organic contaminations on the glass surface, by sol-gel dip coating and chemical vapor deposition (Piispanen & Hupa et al., 2011). Moreover, polymers are coated on variety of surfaces for biomedical applications to obtain antimicrobial surfaces which are toxic to microorganism (Grumezescu & Holban et al., 2014).

Another functional coating method is plating is formed by metals on a conductive surface. There are many applications that use plating as shown in Figure 1.1. Solid surfaces can also be coated with metals such as gold, stainless steel, silver, copper, and nickel by dipping technique. In dipping technique, object is immersed into a solution containing the desired surface material, so coating can be obtained by chemical or electrochemical action. Generally, liquids are preferred and used for plating. Other plating techniques are known as sputter and vapor depositions (Mattox, 1973; web8). Much plating is applying for decorative purposes at the same time the plating is done to prevent corrosion, to resist heat, to reduce friction, to conduct electricity, to enhance appearance, to improve paint adhesion, solderability, wearability and also IR reflectivity for functional purposes (web9; web10)

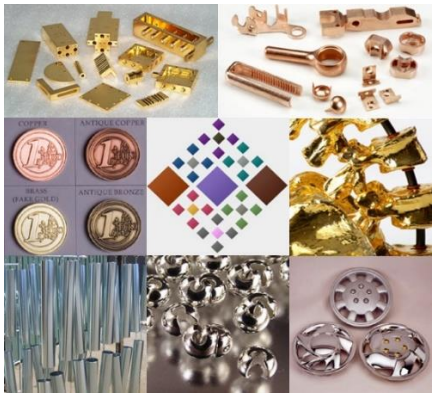

Figure 1.1. The applications of the plating method
(Source: web11)

Optical coatings are another fundamental functional coating type with many application areas. Generally, the optical coating is applied on glasses and especially optical surfaces such as lenses, optical engine and the windscreen in automobile industry (Helsch & Frischat et al., 2004). One of the optical coating is scratch resistant or anti scratch coating. Anti-scratch coating does not change lens functions and affect vision. Usually, the coatings are made of high index polymers such as polycarbonate, poly methyl methacrylate or polysulfone (web12). The anti-scratch coating behaves as a preventive layer which improves mechanical properties and resistance against to minor scratches (Heiting, 2015; TSP, 2012). Anti-scratch coatings are used on the plastics to provide extra resistance to chemical attack, outdoor weather resistance and also optical clarity.

Figure 1.2. Anti-scratch coating
(Source: Heiting, G., 2015)

Another optical coating is known as anti- reflective coating. Thanks to thin multilayer coatings, reflections are cut off from the surfaces of eyeglass lenses, glass panels, window, solar and architectural glasses, also (Chen & Li et al., 2011). Therefore, anti-reflection coatings improve the performance of optical systems by increasing transmission, enhancing contrast and also eliminating the reflection. The anti-reflection coatings are safe, durable and also resistant to chemical, physical and environmental harsh effects (web13). Anti-reflection coating also provides better and more comfortable vision for personal uses with especially lenses. At the same time, the blocking of ultraviolet (UV) light treatment is an important for lens. Generally, the sun's UV rays damage human's skins and eyes. The reasons of many eyes problems like cataracts and retinal damage can be high levels of ultraviolet light exposure (Heiting, 2015). To prevent UV light, a thin film coating can be used (Ozkan & Lee et al., 2002).

In conclusion, all functional coatings can be applied to change the surface properties. Meanwhile, new properties such as electrical conductivity, magnetic and especially optical properties can also be added to surfaces.

1.3. Optical Coating Theory

The optical property is defined as response of a substance or medium which is exposed to electromagnetic radiation, especially visible light. There are interactions between electromagnetic radiation and substances because electromagnetic radiation passes through them. Electromagnetic radiations are described as light, heat, radar, radio waves, and x-rays etc. Each electromagnetic radiation has different frequencies which is called as electromagnetic spectrum. Distributions of electromagnetic radiation are emitted

and absorbed by substances, medium or objects dissimilarly. Therefore, the electromagnetic spectrum, which is the specific ranges of wavelengths of electromagnetic radiations, formed by microwaves, infrared light, ultraviolet light, X-rays and gamma-rays (Callister, 2010). The electromagnetic spectrum is shown in following Figure 1.3.

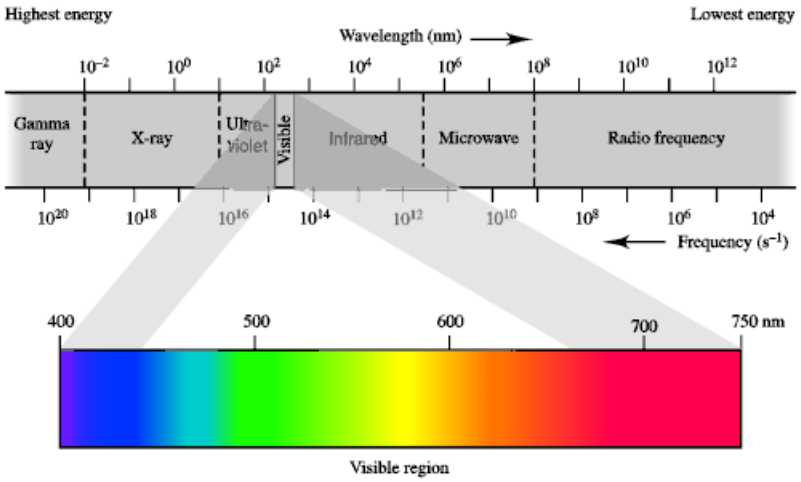

Figure 1.3. Electromagnetic spectrum
(Source: Hunt, D. I., 2015).

According to above electromagnetic spectrum, gamma rays which are emitted by radioactive materials have the shortest wavelengths (< 10^{-2} nanometers), but the highest frequencies. X-rays range from 10^{-2} to 10 nm in wavelengths. X-rays are about the size of an atom. If the range of the wavelength is between 10 and 310 nm, it is called as ultra violet (UV) radiation. Visible light region is the narrowest region with wavelengths ranging between about 400 nm and 700 nm. In visible spectrum region, the colors of the rainbow are perceived and determined by wavelength. The radiation which have 400, 500 and 650 nm wavelengths appear violet, green and red, respectively. The eyes are sensitive to this spectral range. Between the wavelengths of 750 nm and 10^{6} nm show infrared region. Between 10^{6} and 10^{8} nm wavelengths demonstrate microwave region which is separated from the radio waves because they are used in different technologies. The wavelengths of radio waves are longer than 10^{8} nm, so they have the lowest frequency and energy (Callister, 2010; Askeland et al., 2010). Radio waves are emitted by gases. Therefore, radio waves are found everywhere in the universe.

The optical phenomena include that all these electromagnetic radiations and spectrum show the interactions between substances and electromagnetic radiations and also optical behaviors of electromagnetic radiations. In optical phenomena, light

radiations proceed from one medium into another medium. Because of the proceeding of light radiations, some of the light radiation can be transmitted, reflected and absorbed, therefore the optical coating and its theory can be explained with the optical behaviors of the light radiations (Callister, 2010).

An optical coating, which is composed of thin film layers of material deposited on the surface of optical components by using specialized methods, is used to improve the properties of transmission or reflection of the light within optical system (Callister, 2010). Reflection, transmission, absorption, refraction, polarization, and some laws such as Snell and Fresnel, form and explain the basis of the optical coating theory.

Reflection is the process by which the light rays that reach an object and they are returned either at the boundary between the object and its surface or at the interior of the medium of the object, so, the light rays bounce by changing direction or are reflected partially or totally from the object (Roychoudhuri, 2008). The incident light rays are reflected at an angle. These reflected light rays produce clear image, which is called as a mirror image, and this type reflection is good or regular reflection. However, when the light rays reflect on the rough and bumpy surface, the reflected light rays scatter, so poor reflection occurs and it is called as a diffuse reflection. On the contrary reflection, the process of transmission is that the light rays reach and hit the object and they pass through the medium of the object. The transmitted light rays can scatter or produce clear image like reflection, therefore, diffuse and regular transmissions occur, respectively. Furthermore, absorption transform the power of the light rays to another type of energy which is generally heat by interaction with the object. Firstly, the light rays reach the object and these light rays can be absorbed totally and then the absorbed light rays convert into heat (web14). When the light rays go into another new medium at a certain angle, the speed of the light rays changes, so the direction of the light rays also change and the light rays are tilted. This process is called as a refraction (Roychoudhuri, 2008). The behaviors of light ray are shown in Figure 1.4.

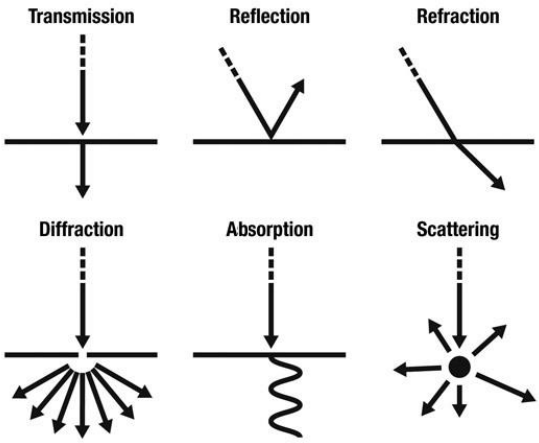

Figure 1.4. The light ray behaviors
(Source: web15).

The amount of bending of the light rays depends on refraction indices between two media, and this situation is defined by Snell's Law. The refraction index, which is shown as 'n', is described that the speed of light in the vacuum medium is divided by the speed of light in the medium. According to the refraction indices of the two-different media or materials, Snell's Law determines the angle of the bending light rays. Snell's Law can be explained in the following figure, the incident light ray reach on an interface between medium 1 and medium 2. This light ray forms the angle between normal to surface and interface because of the reflection and refraction, so the angle formed can be measured. If the refractive index of medium 2, n2, is higher than the refractive index of medium 1, n1, the light ray is transmitted into the second medium by changing direction and bending. Therefore, at the second medium refracted light ray move on with different angle and the Snell's Law state that the following equation and Figure 1.5.;

$$n_1 \, sin\theta_1 = n_2 \, sin\theta_2 \tag{1.1}$$

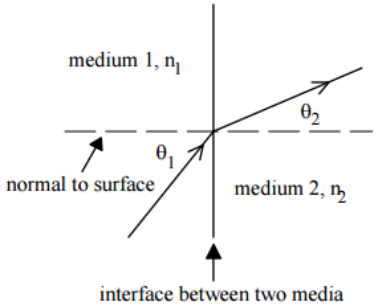

Figure 1.5. Illustration of incident, refracted rays and their angles
(Source: web16)

Another law which explains the optical coating theory is Fresnel Law. Fresnel equations based on Snell's law, electric and magnetic fields of two different media and also polarization. Polarization can be explained as the oscillations of waves with different orientations. Generally, light is an electromagnetic wave which forms electric field and oscillates in the direction of propagation. Light is called polarized if the direction of the electric field of light which do not fluctuate and is well defined (Diem, 2015). The incident light rays form plane which contains the reflected and incident rays while reaching on the reflecting surface. It is called as a plane of incidence. If the electric field of light is parallel to the plane of incidence, it is called as a parallel polarization or 'p' polarization. If the electric field of light is perpendicular to the plane of incidence, it is called as a perpendicular polarization or's' polarization (Roychoudhuri, 2008). The polarizations of the reflected and transmitted rays and also phases describe to the Fresnel equations. In addition to the Snell's Law, to derive the Fresnel equations the electric field of the electromagnetic wave is given by E_i and in the same way interface which separates two media with wave vector k_i at angle θ_i (Lvovsky, 2013). The Fresnel equations are derived for two cases which are s and p polarizations because the electromagnetic waves are transverse. According to p and s polarizations, incident, transmitted and reflected waves, E, H and k vectors and their directions for each of the waves are shown in Figure 1.6.

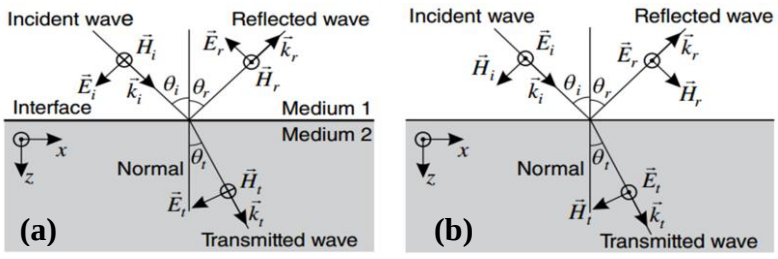

Figure 1.6. a) Field vectors of the incident, transmitted, and reflected waves in case the electric field vectors lie within the plane of incidence (P polarization). (b) Field vectors of the incident, transmitted, and reflected waves in case the electric field ve ctors are perpendicular to the plane of incidence (S polarization) (Source: Lvovsky, 2013).

For optical materials some assumptions are made and Fresnel equations can be derived, and further simplified with the angles of incidence and transmission by integrating Snell's Law (Lvovsky, 2013):

$$r_p = -\frac{\tan(\theta_i - \theta_t)}{\tan(\theta_i + \theta_t)} \tag{1.2}$$

$$t_p = \frac{2\sin\theta_t \cos\theta_i}{\sin(\theta_i + \theta_t)\cos(\theta_i - \theta_t)} \tag{1.3}$$

$$r_s = -\frac{\sin(\theta_i - \theta_t)}{\sin(\theta_i + \theta_t)} \tag{1.4}$$

$$t_s = \frac{2\sin\theta_t \cos\theta_i}{\sin(\theta_i + \theta_t)} \tag{1.5}$$

For optical coatings and optical design, the Fresnel equations are used, so the principles behind Fresnel equations are important to understand.

Nowadays, these laws and polarizations have been utilized for many applications such as polarized sun glasses. Regularly, light is not scattered in all directions, reflected light proceeds in a more horizontally collimated direction, so it means that light reflected from surfaces is polarized horizontally. Thus, irritating and hazardous intensity of light is described as a glare. The effects of glare can be reduced by rotating the polarizer horizontally from reflections (Morgan, 2015).

1.4. Optical Coating Materials and Processes

Applying optical coating theory, the specification of optical coating materials and their methods are important because each material has different coating properties and different methods. In this part, the properties of optical coating materials are defined clearly and also coating methods are explained for these materials.

1.4.1. Optical Coating Materials

The optical coating materials vary with different coating techniques. The physical, electrical, thermal, chemical and optical properties of thin films are influenced by the materials used and fabrication techniques applied.

1.4.1.1. Inorganic Optical Coating Materials

Most commonly used inorganic optical coating materials are fluorides, oxides, nitrides, sulfides, selenides, carbides, and tellurides etc. Fluorides, oxides and nitrides are used widely.

1.4.1.1.1. Fluorides

Fluoride compounds are used in coatings for the UV to middle-IR regions. Fluorides coating materials require high vacuum to form fluoride film layers. Fluorides keep their chemical composition upon evaporation. With thermal evaporation, dissociation does not happen between the fluoride bonds because fluoride bonds are stronger than oxide bonds. Some fluorides and their compositions can absorb water and UV. However, according to depositions made at high temperatures and different conditions, the water absorption bands, UV spectral ranges, mechanical strength and also the index of fluoride films exhibit the variations (Friz & Waibel et al., 2003).

Aluminum fluoride (AlF_3): Aluminum fluoride, AlF_3, is known as a low index optical coating material, it provides resistance and adhesion on coating surface such as anti-reflection coatings. The refractive index of AlF_3, n_{AlF3}, is 1.4 (λ=200 nm) (Friz & Waibel et al., 2003). E-beam and ion assisted deposition (IAD) methods are used for AlF_3 deposition at the high temperatures. AlF_3 does not absorb water, and has good mechanical strength (Heitmann, 1970).

Barium fluoride (BaF_2): Barium fluoride, BaF_2, has low index of refraction of 1.45 (λ=5 μm) material with low solubility in water, but it can provide high transmission. BaF_2 is the most resistant, among the optical fluorides, to high energy radiation and it is more susceptible to thermal shock. There are many variety applications of BaF_2 such as

windows, lenses, biological samples such as liquid cell windows (particularly aqueous solutions) and drilled discs (web17).

Calcium fluoride (CaF_2): Calcium fluoride, CaF_2, is commonly used material for optical coatings because it has high transmission range, low absorption and also low index of refraction of 1.4 (λ=4 μm), so it can be used without an anti-reflection coating for free-space lasers applications. It is resistant to water, chemical and heat and sensitive to thermal shock. CaF_2 can be used up to 1000˚C without moisture, but degradation of CaF_2 occurs in the presence of moisture for temperatures over 600˚C. It has a high mechanical strength therefore it is used at high pressure applications. The deposition of CaF_2 as thin films is performed by using different physical vapor deposition (PVD) techniques such as electron-beam evaporation (EBE), thermal evaporation and magnetron sputtering etc. (Çetin & Korkmaz et al., 2013).

Magnesium fluoride (MgF_2): Magnesium fluoride, MgF_2, is a suitable material for optical coating because it has a low refractive index (varies from about 1.48 to 1.3) coating material and good transmission ranges, so has been also used in anti-reflection coatings like AlF_3, BaF_2, and CaF_2. Magnesium fluoride is a bi-refringence material that means double refraction and according to this property the selection of magnesium fluoride in an optical coating design is an important parameter. MgF_2 is resistance against mechanical and thermal damage effects and is harder than CaF_2 almost twice. However, it is more expensive than BaF_2, and CaF_2. Generally, MgF_2 is used for biological and military imaging applications such as windows, lenses, optical filters, optical beam splitters and wedges. To deposition thin films of MgF_2 thermally physical vapor deposition (PVD) techniques are used (Perales & Herrero et al., 2007).

Lanthanum fluoride (LaF_3): Lanthanum fluoride, LaF_3, has high refractive index (varies from about n = 1.7) and also low absorption unlike other fluorides. Therefore, generally it is used for high refractive index layer. LaF_3, which deposits dense and hard layers by electron-beam evaporation, it can be applied in many applications such as fiber optics, electrodes, and fluorescent lamps (Friz & Waibel et al., 2003).

1.4.1.1.2. Oxides

Oxides are inorganic materials which are important to optical coating, because oxides have a suitable refractive indices and spectral ranges. At the same time, they form films, which have desired properties such as stable and durable due to their hardness and resistance to chemical, mechanical and environmental effects. At high temperatures a lot of oxides react with metals, so the electron beam evaporation method should be used. Another deposition method for oxides materials such as magnetron sputtering, ion beam sputtering, and ion assisted deposition (Friz & Waibel et al., 2003). Some oxides and their properties are explained in below.

Titanium oxide (TiO_2): Titanium oxide, TiO_2, is used for optical coatings. It provides the highest refractive index, approximately between 2.2 and 2.4 at 550 nm. If TiO_2 combines with the other oxides, it can be stable, durable and hard material. Moreover, suboxides (TiO, Ti_2O3 and Ti_3O_5) are also used as for the production of TiO_2 films to avoid evaporation difficulties. To form deposited thin film of TiO_2 beam splitters, cold mirrors and heat-reflecting mirrors, anti-reflection coating, and magnetron sputtering methods are used (Friz & Waibel et al., 2003).

Silicon dioxide (SiO_2): Silicon dioxide, SiO_2, which is known as silica, is an important thin-film optical coating material. It has the low refractive index approximately 1.45 at 550 nm and low absorption material, nevertheless it can be combined with the other high index materials. It is resistant to chemical, mechanical and environmental detrimental effects. It is used in equipment such as standard UV/VIS measurement optics, all-dielectric mirrors, beam-dividers, and polarizers (Bach & Krause et al., 2003). The bulk form of SiO_2 is defined as quartz. On the contrary quartz, SiO_2 thin films are amorphous and by using ion-beam assisted deposition, sputter deposition and high substrate temperature water permeability can be minimized effectively (Friz & Waibel et al., 2003). At the same time, the properties of thin films of SiO_2 can be changed by applying different vapor deposition techniques.

Silicon monoxide (SiO): Silicon monoxide, SiO, is commonly used for multilayer coatings and SiO layers forms Si_2O_3 within oxygen atmosphere, so it can be used for anti-reflection coatings. The refractive index of this layer is around 1.55 (Friz & Waibel et al., 2003). There are many applications for SiO optical coatings such as jewelry, reflectors, mirrors, and flood lamps (Materion, 2015).

Aluminum Oxide (Al_2O_3): Aluminum oxide, Al_2O_3, has a medium refractive index (n=1.63 at 550 nm), low absorption material. It is used in the spectral range between UV (<300 nm) to IR (~5 μm) regions for coatings. It can be used in UV laser anti-reflection coating, polarizer and also dielectric mirror designs (Stenzel, 2014).

Indium oxide (In_2O_3): When indium oxide, In_2O_3, is added to approximately 5-10% Sn, indium tin oxide forms which is called briefly as ITO and is commonly used as a transparent conductive film because of its optical transparency and electrical conductivity. The refractive index of ITO is approximately 1.95 at 550 nm. It can be deposited as thin film. However, the optical and electrical properties of ITO films are dependent on the deposition method and parameters (Friz & Waibel et al., 2003). ITO thin films include high density of charge carrier because of its conductivity. High conductivity is connected to high transmission in the spectral region. Physical vapor deposition is applied to occur deposition of thin films of ITO. Generally, ion assisted and electron beam evaporation and also sputter deposition techniques are used for ITO thin films (Sok Won & Manil et al., 2011).

1.4.1.1.3. Nitrides

In addition to fluorides and oxides, nitrides such as aluminum nitride, barium nitride, magnesium nitride and silicon nitride etc. are used for inorganic optical coating materials. However, the most commonly used nitride material is silicon nitride (SiN_x).

Silicon nitride (SiN_x): The most important of Silicon nitride, SiN_x, is Si_3N_4 that is deposited on the surface to form thin films which are suitable as antireflection coatings because of the optical properties. Depending on the deposition method and parameters, Si_3N_4 can have a wide range of refractive indices between 1.8 and 2.1. Thin films of Si_3N_4 can be used for Si wafer solar cells since it includes a high amount of hydrogen. It is resistant to thermal effects and also durable at high temperature. There are many deposition methods for Si_3N_4 films, but generally, physical vapor deposition technique (PVD) is applied. Magnetron sputtering, dual ion-beam sputtering, and ion assisted thermal evaporation can be given as PVD examples (Ku & Lee et al., 2010).

1.4.1.2. Organic Optical Coating Materials

Organic materials are obtained as thin films by applying different techniques such as ion assisted evaporation deposition, ion beam sputtering, chemical vapor deposition, spin and dip coatings. Some organic materials have excellent optical properties such as low absorption, high refractive index and also low optical haze. At the same time, organic materials have high mechanical flexibility, electrical permeability and chemical activity, and also the mechanical stability of organic materials may be improved. Because of these properties, some organic materials are used for optical coating (Piegari & Flory et al., 2013). The most commonly used organic optical coating materials are transparent acrylates, polyesters, polyvinyls and polyamides.

1.4.1.2.1. Acrylates

Acrylates are the most commonly used for protective coatings because they have good electrical insulation properties and environmental resistance, and also they can protect against moisture. They are known as thermoplastic polymers which have optical characteristics. Acrylic coatings are used in many optical applications such as lenses, decorative household items and also light fixtures. The refractive index of acrylates is approximately 1.48. Therefore, their coatings have high light transmittance. Acrylates are sensible to organic solvents such as esters, ketones, fluorinated and chlorinated solvents etc., so the coatings can be dissolved and removed by using solvents (Licari, 2003). Some acrylate polymers are poly methyl acrylate (PMA), poly ethyl acrylate, poly ethyl hexyl acrylate, poly butyl acrylate, poly butyl methacrylate and poly methyl methacrylate (PMMA).

1.4.1.2.2. Polyesters

Polyesters can be separated into two types as saturated and unsaturated polyesters. Generally saturated polyesters are used for paints and coatings as binders. The properties of them vary with their molecular weight. High molecular weight polyesters are thermoplastic polymers which show better solubility in solvents and are used for highly flexible coatings with good surface hardness and stability. Moreover, polyester coatings exhibit very good impact, stain and scratch resistance, and also exhibit good environmental and chemical resistances. However low molecular weight polyester are not suitable satisfactory film formers for coatings (Tracton, 2006). Polyester coatings are used in insulations, electronic and computer assemblies. To provide these characteristic properties polyesters can be modified with styrene, phenolic resins or silicones etc. (Licari, 2003).

1.4.1.2.3. Polyvinyls

Polyvinyls are known as the oldest polymer type which include many structural variations. They are generally applied for protective and electrically insulation coatings polyvinylidene chlorides and fluorides and also polyvinylaldehydes are given as examples (Licari, 2003). Moreover, these polyvinyl coatings are used as especially moisture barriers, anti-fog coating and also wire insulation. These coatings have resistance to abrasion, tough and good adhesion properties (Tracton, 2006).

1.4.1.2.4. Polystyrenes

Polystyrenes are used for optical coating and electronic applications at moderate temperatures. They have high dielectric strength and resistivities, therefore, polystyrenes are preferred for capacitors. Another important property of polystyrenes is transparency, but they have coloring property, so transparent, translucent and opaque colors of polystyrenes are used decoratively. Moreover, their refractive indices (n=1.60) are suitable for optical coating, therefore they are often used in lenses and optical equipment (Licari, 2003).

1.4.2. Optical Coating Production Processes

Vapor deposition can be described as a production process which transforms materials in vapor state to solid state by condensation or chemical reaction for coating mostly the surfaces. There are two main vapor deposition processes these are physical vapor deposition (PVD) and chemical vapor deposition (CVD). In addition to these deposition techniques, dip and spin coating techniques can be used as wet coating for optical system. These coating techniques and their different types will be explained in following parts.

1.4.2.1. Physical Vapor Deposition (PVD)

PVD techniques provide high quality optical coatings. In PVD the coating material transfers into the vapor phase, so PVD techniques are separated into two main groups as evaporation and sputter techniques (Piegari & Flory et al., 2013). In PVD methods metals, polymers, alloys, ceramics, glass etc. are used as substrate materials and also generally inorganic materials such as metal oxides, carbides, nitrides, sulfides, selenides, tellurides etc. are deposited on the substrate as coating materials. With PVD methods good coating adhesion and excellent abrasion resistance can be provided. However, some PVD method have low deposition rates, and require vacuum to deposit thin film. Thin films produced by using PVD methods are used in many applications such as optical, magnetic, optoelectronic and microelectronic equipment because these thin films provide protection against corrosion and insulation against heat (Bergauer, 1993). The application of PVD technologies at large scale, reduce the hazardous waste generated with high volume operations.

1.4.2.1.1. Evaporation

One of the thin film physical vapor deposition techniques is evaporation. Vapor which are provided by vacuum proceed to substrate and condenses on the substrate as solid. Therefore, to evaporate the material to be deposited, an energy source is required. There are many different energy sources such as thermal, electron beam and ion beam assisted.

Thermal Evaporation: In thermal evaporation, the vapor is produced by means of heat release that is generated by electrical current passing through a simple resistive heat element or filament. These filaments which have different configurations are known as boats. These boats which are made from thin sheet metal pieces such as tungsten, tantalum and molybdenum are suitable for high temperatures, and also hold small amounts of coating materials. During the coating process, a high current is passed through the boat, the coating materials are vaporized in vacuum. Therefore, the free atoms or molecules move through a very long mean free path. Vapor molecules can reach the substrate at the top of the chamber, condense onto the substrate to form a thin film as a solid state (Tracton, 2006; MacLeod & Macleod et al., 2010). A scheme of the thermal evaporation deposition equipment is showed in the Figure 1.7.

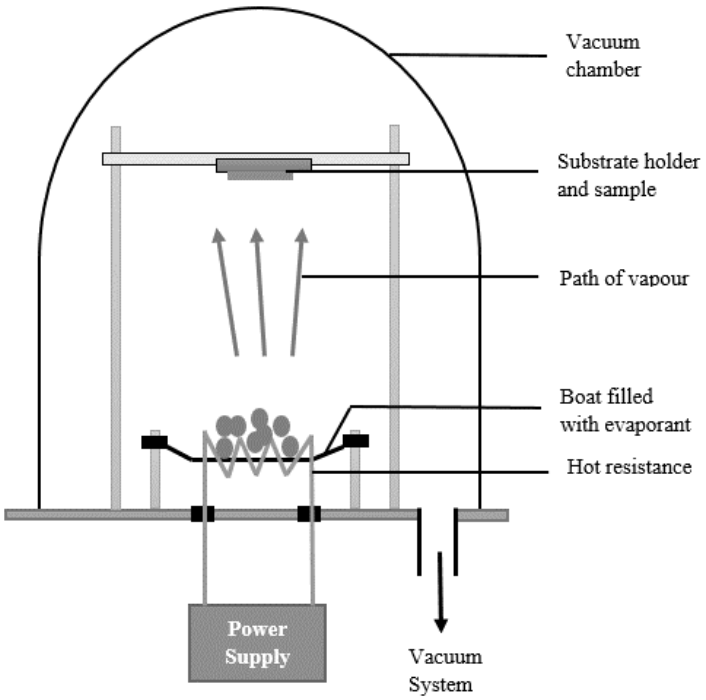

Figure 1.7. Schematic diagram of thermal evaporation system.

As demonstrated above evaporation system, required equipment can be listed such as the chamber together with pumps, substrate holder, boat, power supply to melt the evaporant for the thermal evaporation deposition. In above vacuum chamber, the vapor spread towards substrate in straight lines, so the film is formed smoothly, and thickness of the film depends on the position and orientation of the substrate according to the vapor source. Cleanliness of the substrate surface, incidence of the vapor stream and temperature range of the substrate are critical parameters. The evaporation is realized in a vacuum chamber that is evacuated to a pressure usually of 10^{-5} mbar (approximately 10^{-3} Pa). If the pressure of vacuum is close to atmospheric pressure or not at desired value, non-uniform thin film is produced as a result of insufficient evaporation (MacLeod & Macleod et al., 2010).

Electron Beam Evaporation: In electron beam evaporation heat is produced by electron beam or e-beam bombardment on the substrate to be deposited. This process is similar to the thermal evaporation. In e-beam evaporation coating material is heated and evaporated to form a thin film on the surface of the substrate by the evaporated atoms. E-beam evaporation method has much more benefits than the thermal evaporation because e-beam evaporation adds a larger amount of energy into the coating material, so high density film is formed and good adhesion to the substrate is provided. At the electron beam evaporation, the degree of the contamination is lower than thermal evaporation because of the fact that the electron beam only heats the coating material not the entire melting pot. The electron beam is produced by an electron gun. Accelerated and emitted electrons move towards the anode by high voltage (usually 10 kilovolts). The crucible can be defined as the anode. To bend the electron trajectory, a magnetic field is applied. E-beam evaporation is also performed within the vacuum chamber (Tracton, 2006; Piegari & Flory et al., 2013). The following Figure 1.8 exhibits a diagram of the electron beam gun evaporation.

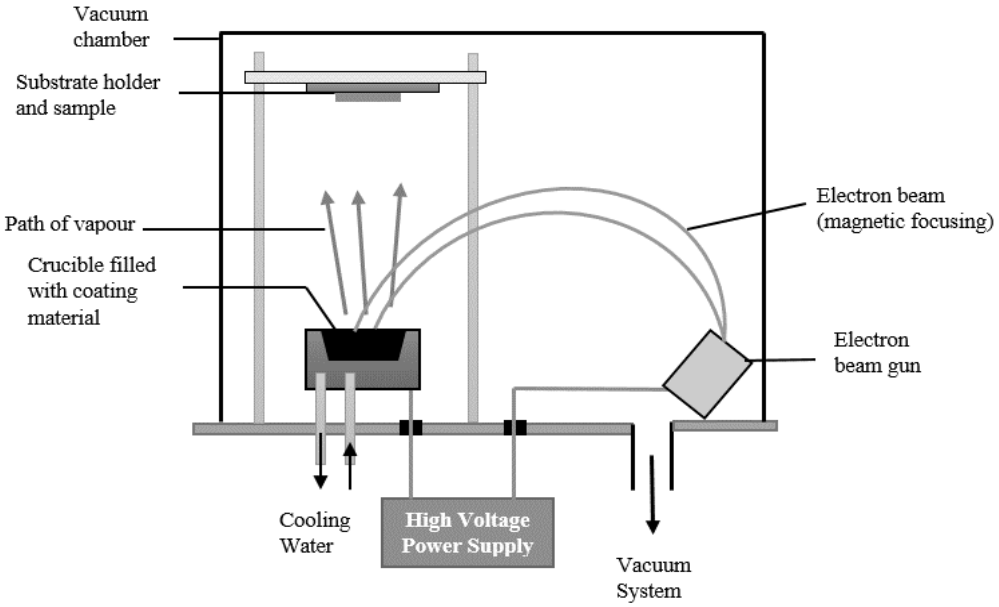

Figure 1 8. Schematic diagram of electron beam evaporation system.

Electron beam evaporation techniques are used in many industries such as aerospace industries for thermal barrier coatings, tool industries for hard coatings, and semiconductor industries for electronic and optical films. Thin films are usually porous because they are deposited by electron beam evaporation technique. However, to obtain less porous or nonporous thin films, another evaporation technique, ion assisted evaporation technique, is applied (Stenzel, 2014).

Ion Assisted Evaporation: For ion assisted evaporation deposition (IAD) system ion source is added to the electron beam evaporation system, so fundamentally IAD is a modified e-beam evaporation technique. During deposition, film is bombarded by ion beams which have high energy (Stenzel, 2014). Generally, IAD is performed at low temperatures, however, it provides higher molecular density and the lowest absorption in the thin film, because of that refraction index increase noticeably. The added ion sources can be used to pre-clean or etch the surface of the substrate to improve adhesion. Moreover, high energy ions can be used for producing more durable and stable coatings. The deposition process occurs in the vacuum system and on the hot substrate. IAD is used for microelectronics, semiconductors and telecommunications applications (Griot, 2015).

Sputtering: Sputtering is based on the momentum principle, formed by the collision of the atoms or molecules. Sputtering is a process which occurs when material is removed and ejected from target by exchanging momentum between the target and the gas atoms in a vacuum chamber. Silicon wafer is generally used as a substrate. Molecules

or atoms are removed from a target by high energy molecules or particles. From the particles to the surface atoms the momentum is transferred, so atoms take enough energy to escape where are placed on the surface. These ejected atoms from target (cathode) move towards the substrate and are deposited as a thin film (Tracton, 2006). An inert gas is used as a sputtering gas such as argon and generally light element such as neon is preferable for efficient momentum transfer (Wilson, 2012). Figure 1.9 shows a schematic diagram of sputtering deposition system.

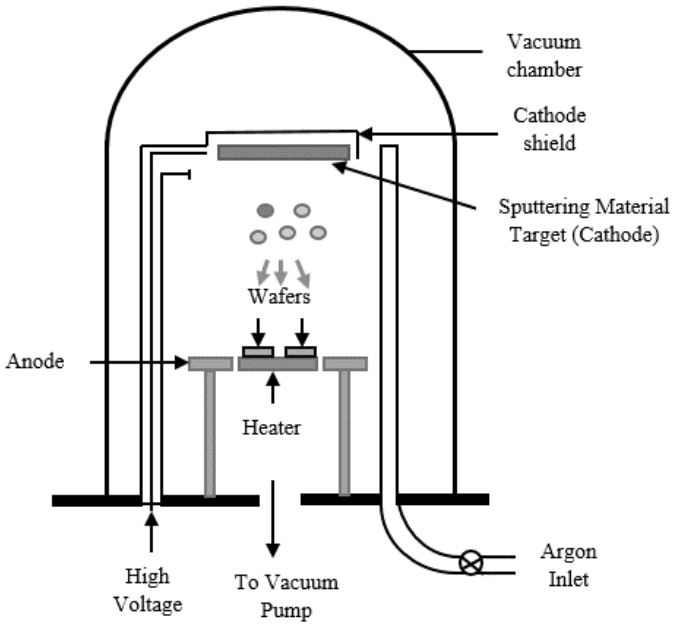

Figure 1.9. Schematic diagram of sputtering deposition system.

The required energy for sputtering is less than 1000 eV. This situation reduces the safety risk of high voltages and the load on the power supply (Tracton, 2006). Sputtering can be used for multilayer optical coatings, and for metal targets that are electrically conducting. As target materials alloy, mixture or pure metal, ceramic, oxide, nitride, boride, carbide, etc. can be provided (MacLeod & Macleod et al., 2010). Sputtered hin films have good adhesion than the other physical vapor deposition techniques. Sputtering is used commonly in many applications such as semiconductor, anti-reflection and wear resistance coatings and also transistors (Tracton, 2006).

1.4.2.2. Chemical Vapor Deposition

Chemical vapor deposition (CVD) is one of the most common processes for thin film fabrication. CVD is widely applied for optical thin film coatings. In CVD processes, a very wide range of inorganic materials such as nitrides, oxides, carbides and also organic polymers such as acrylates and fluorinated polymers are used (Seshan, 2001). CVD enables low temperatures synthesis of simple or complex compounds (Bach & Krause et al., 2003). By controlling CVD process conditions, physical and chemical properties of the films can be tuned. CVD process is performed in a vacuum chamber under moderate to high vacuum. Precursors are introduced to deposition chamber ın vapor forms. Substrates are usually heated to improve surface mobility of species. Thermal, photocatalytic or spontaneous initiation of chemical reactions can happen in gas phase and on the substrate surface. CVD is a suitable process for fabrication of conformal coatings in flat and porous substrates (Bach & Krause et al., 2003). Derivatives of the CVD processes are metal-organic chemical vapor deposition (MOCVD), atomic layer deposition (ALD) and initiated chemical vapor deposition (iCVD), plasma enhanced chemical vapor deposition (PECVD), hot-wire chemical vapor deposition (HWCVD) and photo-initiated chemical vapor deposition (PICVD).

Metal- organic chemical vapor deposition (MOCVD) or less commonly organo-metallic chemical vapor deposition (OMCVD) is used to produce thin layers of semiconducting materials by organometallic compounds as precursors. By using MOCVD process generally, single, polycrystalline or amorphous thin films are obtained. In most cases, MOCVD is an important process for opto-electronic and high speed electronic devices such as lasers, photodetectors, solar cells, phototransistors, photocathodes and field effect transistors. Semiconducting compounds, alloys and hydrides are also used in MOCVD process. These materials are dimethyl cadmium ($(CH_3)_2Cd$) or trimethyl gallium ($(CH_3)_3Ga$, gallium arsenide (GaAs), indium phosphide (InP) and their derivations as the metal source and, ZnSSe and HgCdTe as alloy, arsine (AsH_3) and phosphine (PH_3) as hydrides or an organometallic such as trimethyl antimony (TMSb) or dimethyl tellurium (DMTe).

In MOCVD, the heated organic gas molecules are injected into the reactor and these molecules decompose on the surface of the substrate, which is heated by heater, without the oxygen. This process is called as a pyrolysis. Atoms which are interacted with

surface are released on the surface of the substrate, so these atoms bond to the surface of the substrate and thin layers are obtained at the surface. Generally pressure is approximately 0.5-100 Torr in MOCVD system. Properties of the films can be changed at an atomic scale, that is, the coherences between the structure of the layers and the substrate are obtained and high quality materials are formed because of variation of the vapor pressure and the composition of the gases. Therefore, in MOCVD system the vapor pressure and concentrations of MOCVD materials are significant parameters to find out the deposition rate (Seshan, 2001). Figure 1.10 shows a schematic diagram of MOCVD.

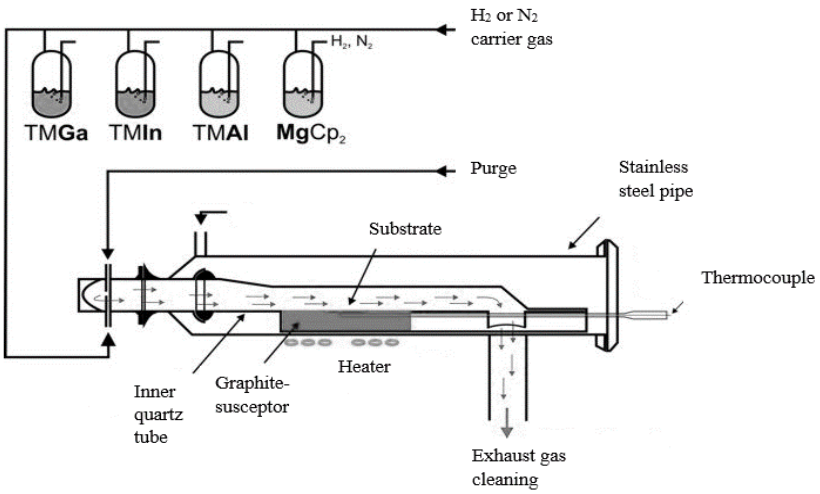

Figure 1.10. Schematic diagram of metal-organic chemical vapor deposition (MOCVD) system.

Another optical coating deposition process is atomic layer deposition (ALD). ALD process is also similar to the conventional CVD. However, ALD process has great benefits like conformity, control of thickness and material composition over alternative deposition methods. Major oxides such as Al_2O_3 and CaO, carbides such as TaC and TiC, fluorides such as CaF_2, LaF_3 and MgF_2, nitrides AlN and GaN, and also polymers such as PMDA–ODA and PMDA–DAH coating materials are used in ALD (Stenzel, 2014). The schematic diagram of ALD is shown in Figure 1.11.

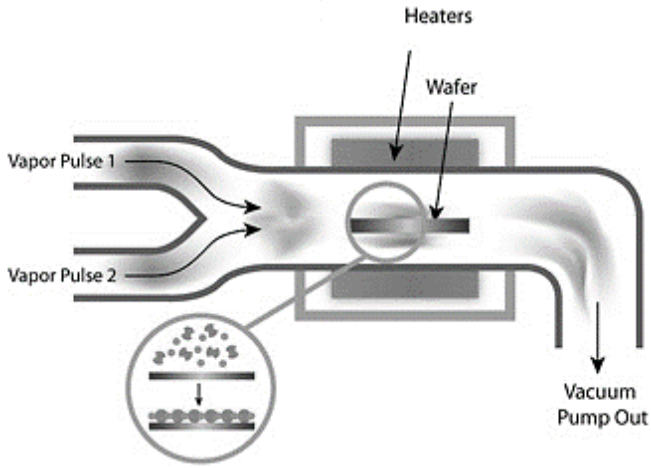

Figure 1.11. Schematic diagram of atomic layer deposition (ALD) (Source: web18).

According to illustrated ALD process, alternating pulses of gaseous chemical precursors are involved and these precursors react with the surface of the substrate. The precursor is injected into the chamber under vacuum (<1 Torr). The precursor reacts with the substrate surface and then purging is performed with inert carrier gas such as N_2 and Ar to remove by-products and impurities. The process is repeated as necessary cycling precursors. This process is then cycled up to obtain desired thickness. ALD processes are performed at modest temperatures (<350˚C). ALD thin-films are used for industrial applications such as sensor, LED, solar cells, thin film batteries and microelectromechanical systems (Johnson & Hultqvist et al., 2014)

One of the newest chemical vapor deposition process is initiated chemical vapor deposition (iCVD) process. In these process, organic and inorganic polymer thin films can be deposited onto a variety of substrates at room temperature. Polymerization mechanism is very similar to solution based free radical polymerization. Radical generation requires either thermal, plasma or photo initiation. All of three initiated CVD techniques can be considered as nanoparticle coating system because nanoparticles have high surface energy (Dorval Dion & Tavares et al., 2013). Hot-wire (filament) chemical vapor deposition (HWCVD) is considered as conventional CVD process and is based on initiation of monomers thermally. Hot wire chemical vapor deposition is also known as catalytic (Cat-CVD). HWCVD is applied for both inorganic and organic (polymers) materials (Schropp, 2009). Inductive heating, infrared radiation, or electrical resistivity can be used as a heat source. A typical HWCVD system is shown in Figure 1.12.

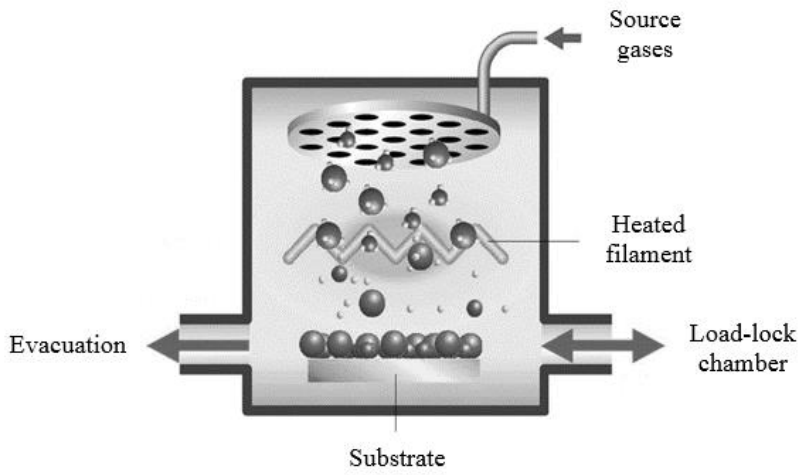

Figure 1.12. Schematic diagram of hot-wire chemical vapor deposition (Source: Matsumura, 2007).

In HWCVD system, the molecules which exit from the source gases collide with the filament surface and radical can be produced by this collision. Therefore, the colliding molecules are atomized by the hot filament and then on the substrate these molecules are deposited uniformly to produce a thin film (Schropp, 2015). Generally, HWCVD process is used in applications such as semiconductors, thin film silicon solar cells, silicon nitride for passivation, encapsulation and isolation, thin film transistors and protective coatings for optical coatings (Dorval Dion & Tavares et al., 2013).

One another chemical deposition process is plasma enhanced chemical vapor deposition (PECVD). For the production of optical coatings PECVD process is commonly used. In PECVD process vapors and gases reach the surface of the substrate and they condense back to solid state then thin film layer can be obtained like other CVD types. PECVD is similar to the standard CVD process (Piegari & Flory et al., 2013). CVD and PECVD can be performed with the same precursors. CVD process occurs at high temperatures, so the deposition of CVD process is controlled by thermodynamic processes. However, PECVD processes happens at lower temperatures than the CVD process, so the deposition of PECVD processes is controlled by the reaction kinetics. This situation has benefits for some substrate materials such as polymers which are sensitive for high temperatures and can be coated easily (Tracton, 2006). By using PECVD process, good deposition rates and denser films can be obtained. The most widely used method for generation a plasma is electric fields ranging from low frequency in kHz region to microwaves frequency in the GHz region. Another plasma source is sputter magnetron. By using magnetic fields, the plasma density can be increased. Usually RF, direct current

(DC) or microwave are used as a power supplies. The pressure range in PECVD system is between 0.01 and 10 Torr (approximately 10^{-2} to 10 mbar) and PECVD is performed in a reactor at temperatures approximately 400˚C (Piegari & Flory et al., 2013). A typical PECVD system set-up is shown in following Figure 1.13.

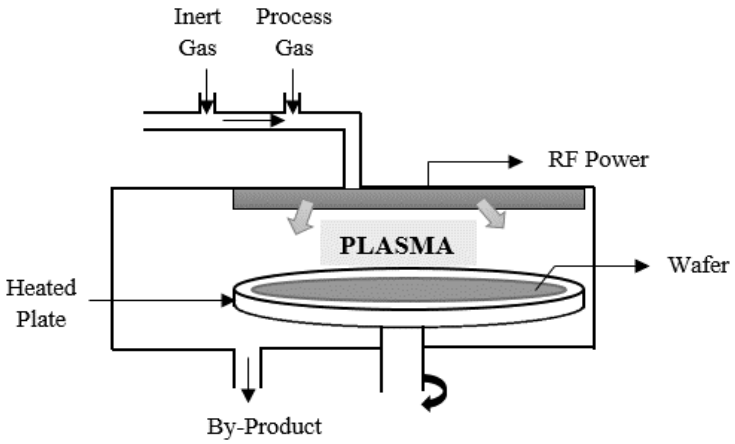

Figure 1.13. Schematic diagram of plasma enhanced chemical vapor deposition (PECVD) system.

Another chemical vapor deposition process for production of optical thin film is photo-initiated chemical vapor deposition (PICVD). In PICVD process, UV light is used to initiate the polymerization reaction by generating radicals. PICVD process is similar to iCVD as a technique. One of the most advantageous is that the energy consumption of PICVD is low. The initiation is introduced by UV light, so the reactant gas mixture has to be photosensitive. In PICVD process materials such as styrene derivatives, acrylic derivatives, methacrylic derivatives, vinyl halides, vinyl esters, vinyl ethers, and vinyl heteroaromatics can be used (Chan & Gleason et al., 2005). Figure 1.14 illustrates a PICVD system.

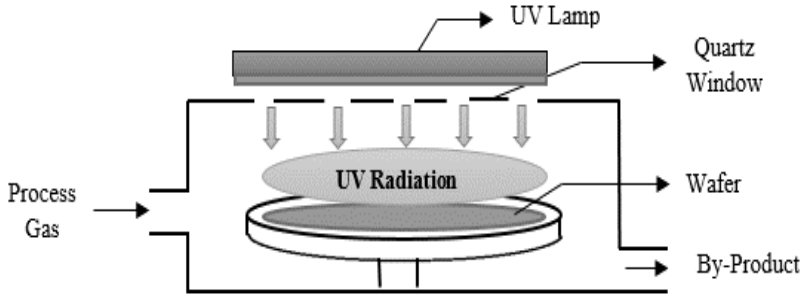

Figure 1.14. Schematic diagram of photo-initiated chemical vapor deposition (PICVD) system.

In PICVD system high deposition rates are possible. However, for PICVD system transparent to walls of the reactor must be transparent to UV light. Compounds which are polymerized tend to stick to window of the reactor which is usually made of quartz (Dorval Dion & Tavares et al., 2013).

1.4.2.3. Other Coating Processes

Other optical coating processes are wet chemical deposition techniques such as dip and spin coatings. In these techniques, materials are in liquid medium. By applying these techniques, high quality optical coatings are obtained homogeneously. Generally, after performing these processes, curing is applied depending on coating solution. Therefore, coating solutions are critical to get highly homogeneous coating with desired optical properties and thickness. For example, the solubility should be very high and also should have quite small contact angle for high wettability. In addition, the solution should be durable and stable. Wet chemical deposition techniques are used in many applications such as transparent conductive coatings, metallic mirrors, and also surface protective coating.

Dip coating is one of the wet chemical deposition techniques which is an industrial coating process. The dip coating technique is performed to get high optical quality thin films. Actually, this method has some advantageous because it is very simple and cheap. Another advantage is that it does not need vacuum system and high temperatures. Dip coating is applied step by step. First of all, the clean substrate is immersed in the liquid coating solution, and withdrawn with a certain velocity under atmospheric conditions. While it is pulled up, thin film layer is obtained on the substrate. The velocity is adjusted properly because the thickness of the thin layer film depends on the velocity. Then excess solution drain from the surface of the substrate and finally the solvent evaporates from the liquid solution. The quality obtained thin film is affected by environmental conditions (Al-Dahoudi, 2003). Dip coating process is shown by Figure 1.15.

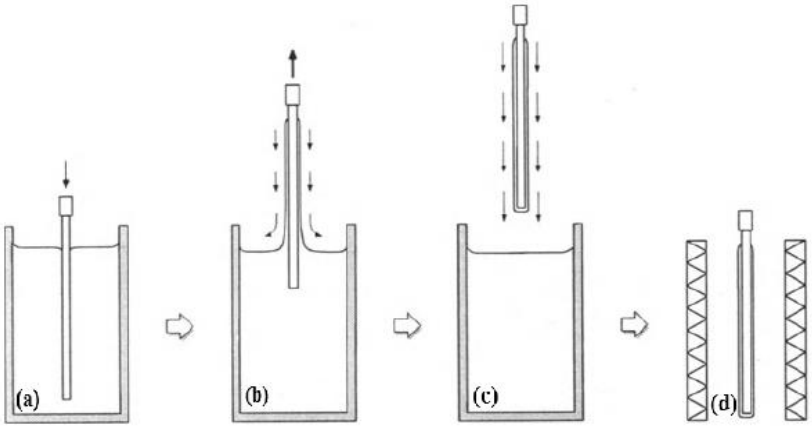

Figure 1.15. Stages of the dip coating process: (a) dipping of the substrate into the coating solution, (b) wet layer formation by withdrawing the substrate, (c) the thin film layer deposition by drainage, (d) the solvent evaporation by curing (Source: Aegerter & Mennig et al., 2004)

In dip coating process, the thickness of film is affected by several forces such as the gravity force, viscous drag, the inertial force and also surface tension. To calculate the thickness of the thin film layer following equation is used:

$$h = c\frac{(\eta U)^{2/3}}{\gamma^{1/6}(\rho g)^{1/2}} \tag{1.6}$$

In Eq. 1.6, the final liquid film thickness is defined as h for pure liquids by the Landau- Levich equation in Eq. 1.6 where c is a constant as 0.944 for generally Newtonian liquids. η denotes the liquid viscosity, U the withdrawal velocity, ρ the liquid density, and γ the surface tension of the liquid against air. Eq. 1.6 shows that the thickness of the thin film increase with increasing withdrawal velocity (Aegerter & Mennig et al., 2004). Dip coating protects against corrosion, and it provides resistivity and durability. There are many applications for dip coating including hand tools, medical instruments, electrical equipment and also anti-reflection optical coating.

Another wet chemical deposition technique is a spin coating. Spin coating technique, which is a simple and widespread process, is applied to produce thin films in many applications. The substrate is placed on a rotatable fixture by using vacuum and the coating solution, which is generally polymer solution, is dispensed onto the surface of the substrate. Thanks to the spinning, the solution is expanded and while the solvent of the solution is evaporating, the uniform coating is formed on the surface of the substrate

(Aegerter & Mennig et al., 2004). The schematic of the spin coating process is shown in Figure 1.16.

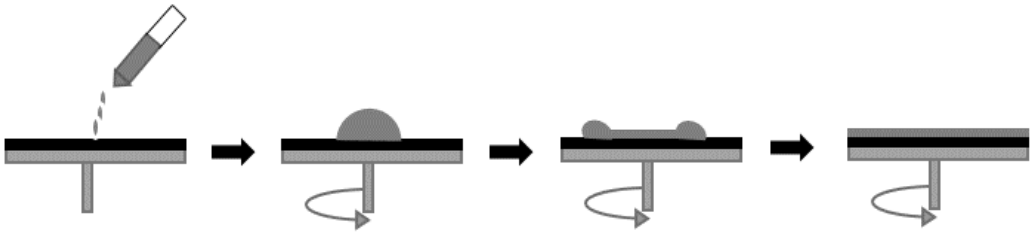

Figure 1.16. Schematic diagram of the spin coating process: dripping solution on the surface, spin up, spin off and thin film formation by solvent evaporation.

In spin coating process, with rotation of the substrate the viscous drag forces act on the film. Film thickness depends on a few parameters including density, viscosity, rotation rate, concentration, evaporation rate of the solvent etc. The thickness of the final film can be calculated in following formula:

$$h_f = x\left(\frac{(C\sqrt{\omega})}{2(1-x)\frac{\rho\omega^2}{3\eta}}\right)^{1/3} \tag{1.7}$$

In Eq. 1.7, h_f is defined as the final thickness of the thin film, ρ is the solution's density, η is its viscosity, ω is the rotation rate, x is the effective solids content of the solution and C is a proportionality constant which depends on the airflow. The evaporation and viscous flow rates depend on rotation of the spin coater. Generally, the spin coating process is applied in inorganic electronics, nanotechnology and also semiconductor industries (Aegerter & Mennig et al., 2004).

When all optical coating processes are evaluated with their all characteristic features, CVD processes especially iCVD technique is the most suitable for conformal thin-film polymeric coatings on a variety of substrates with high deposition rates in a solventless low temperature, low cost process (Spee & Rath et al., 2013).

1.5. Initiated Chemical Vapor Deposition (iCVD) Process

Initiated chemical vapor deposition (iCVD) process has been developed as a subset of hot wire chemical vapor deposition (HWCVD) process. While HWCVD can be used for polymeric film deposition, undesired side effects (chemical reactions) occur due to high filament temperature. In iCVD process, initiator precursor which decomposes thermally at low filament temperature is used to avoid unwanted side reaction in the gas phase. The polymerization occurs at the substrate surface by reaction of radical formed by thermal decomposition of initiator and monomers adsorbed on the surface (Spee & Rath et al., 2013). iCVD process has been developed in the laboratory of Prof. Karen Gleason at the Massachusetts Institute of Technology (MIT). The initiator and monomer(s) are sent to the vacuum chamber at controlled flow rates by using mass flow controllers. The pressure of the vacuum chamber is between 1 mTorr and 10 Torr. The initiator decomposes on heated filaments between 200 and 400 °C.

The mechanism of iCVD can be described in three important steps: (1) the initiator vapor phase decompose thermally to produce radicals, (2) diffusion and adsorption process radical and monomers onto the surface and (3) polymerization via initiation, propagation, and termination on the surface as shown in Figure 1.17.

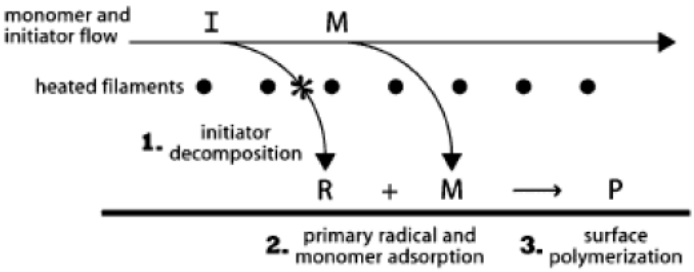

Figure 1.17. Reaction mechanism proposed for iCVD polymerization
(Source: Lau & Gleason et al., 2006)

In Figure 1.17, initiator, radical, monomer and polymer are defined as I, R, M and P, respectively. The three steps of the process are explained clearly in below.

Gas phase reactions

Initiator decomposition: $I\ (g) \xrightarrow{k_d} 2R\cdot\ (g)$ (1.8)

Gas-to-surface processes

Primary radical adsorption: $R\cdot\,(g) \xrightarrow{k_{ad,R}} R\cdot\,(ad)$ (1.9)

Monomer adsorption: $M\,(g) \xrightarrow{k_{ad,M}} M\,(ad)$ (1.10)

Surface reactions

Initiation: $R\cdot\,(ad) + M\,(ad) \xrightarrow{k_i} M_1\cdot\,(ad)$ (1.11)

Propagation: $M_n\cdot\,(ad) + M\,(ad) \xrightarrow{k_p} M_{n+1}\cdot\,(ad)$ (1.12)

Termination: $M_n\cdot\,(ad) + M_m\cdot\,(ad) \xrightarrow{k_t} M_{n+m}\,(ad)$ and $M_n\,(ad) + M_m\,(ad)$ (1.13)

Primary radical termination: $M_n\cdot\,(ad) + R\cdot\,(ad) \xrightarrow{k_t'} M_n\,(ad)$ (1.14)

Primary radical recombination: $R\cdot\,(ad) + R\cdot\,(ad) \xrightarrow{k_t''} R_2\,(ad)$ (1.15)

The free radical polymerization is occurred in this iCVD system which is demonstrated as a schematically in Figure 1.18.

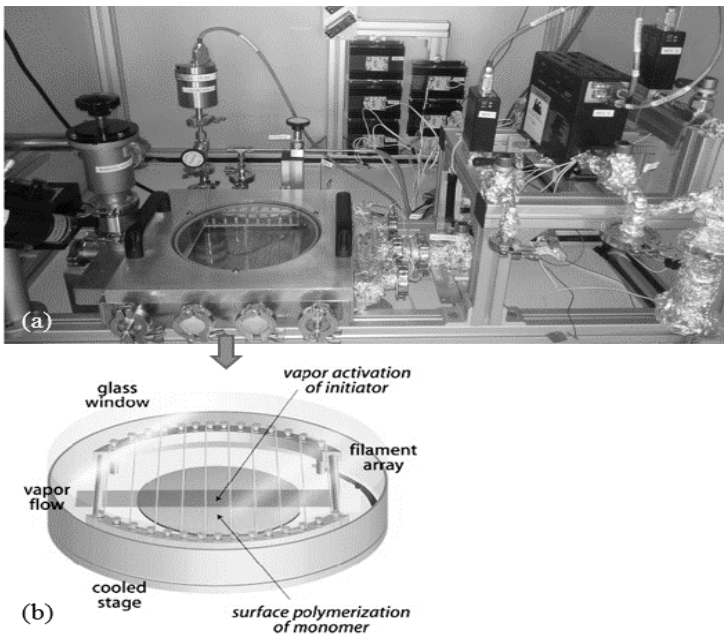

Figure 1.18. A photo (a) and a schematic (b) representation of the iCVD reactor setup for coating on the surface of the substrate (Source: Lau & Gleason et al., 2006)

Figure 1.18 shows iCVD system used in this study. The substrate is cooled to promote adsorption of species and quartz top plate is used monitor deposition process and enables using laser interferometry for in-situ thickness measurements.

Initiator enters the system in vapor phase and decomposes on heated filament surface to form radicals (Eq. 1.8). To provide good adsorption cooler is used at the back side of the reactor, and radicals generated on the filament surface spread out to surface and become adsorbed (Eq. 1.9). The heated monomer molecules are also adsorbed like radicals onto the surface (Eq. 1.10). The initiation step of the polymerization, which is defined as the attack of the radicals on monomer molecules, occurs at the surface (Eq. 1.11). Polymerization proceeds by the addition of the monomer units to each other (Eq. 1.12). The termination step of the polymerization can be either coupling (recombination) or disproportionation (Eq. 1.13). If the polymer chains terminate by the transfer of a hydrogen atom from one radical chain to another by the attack of a radical on a polymer radical, that is known as primary radical termination and disproportionation (Eq. 1.14). If the primary radicals recombine with each other that is also known as coupling (Eq. 1.15) (Lau & Gleason et al., 2006).

When the surface reactions are considered, some kinetic equations are relevant to the polymerization rate, R_p, the kinetic chain length, ν, and the initiation rate, R_i, can be derived. The polymerization rate, R_p, is defined as the rate of monomer consumption, and the initiation rate, R_i, is described as the rate of transferring radicals from initiator molecules to the monomer units. The kinetic chain length, ν, is defined as the ratio of the rate of polymerization to the rate of initiation. It means that kinetic chain length is calculated by means of the consumed average number of monomer units for each radical initiator (Allcock & Lampe et al., 2003). These equations are explained in below (Spee & Rath et al., 2013):

$$R_p = -\frac{d[M]}{dt} = k_p[M][M\cdot] \tag{1.16}$$

$$R_i = k_i[M][R\cdot] \tag{1.17}$$

$$\upsilon = \frac{R_p}{R_i} = \frac{k_p[M][M\cdot]}{k_i[M][R\cdot]} \tag{1.18}$$

Where [M] is the monomer concentration, [M·] is the polymer radical concentration and [R·] is the primary radical concentration. $\overline{DP}$, which is defined as the average number of monomer molecules per polymer molecules. The mole fraction of polymer having DP of n is denoted by X_n which is the number average degree of polymerization. The number average molecular weight, M_n, is obtained from X_n with representing equation below (Allcock & Lampe et al., 2003):

$$X_n = \frac{2\upsilon}{(2-a)} \tag{1.19}$$

$$M_n = MW_M X_n \tag{1.20}$$

Given in Eq. 1.19 and Eq. 1.20, the kinetic chain length is affected by the number-average degree of polymerization, X_n, and the number average molecular weight, M_n. While in Eq. 1.19 a is defined as the fraction of polymer radicals which terminate by recombination, (1 - a) is also fraction of the polymer radicals which terminate by disproportionation and MW_M is the molar weight of the polymer repeat unit (Allcock & Lampe et al., 2003).

Both the initiation rate, R_i, and polymerization rate, R_p, affect the deposition rate of the polymer. Based on Eq. 1.18, while the initiation rate, R_i, is increased, the deposition rate is increased and the average chain length of the polymer is decreased. The increase of the initiation rate causes undesirable situation. Therefore, the increment of deposition rate depends on the rising of the rate of polymerization, R_p. In Eq. 1.16, R_p depends on the monomer concentration, [M] and the polymer radical concentration, [M·], at the surface. Therefore, when the deposition rate is increased without decreasing the average chain length, the monomer surface concentration is required to be increased. It means that the increments of the average chain length and the monomer surface concentration increases the deposition rate of polymer. Actually, the deposition rate also depends on the reaction rate constant, k_p, in Eq. 1.16. Therefore, the reaction rate constant is also dependent on the monomer which is used in the reaction and on the surface temperature. To summarize, when the substrate temperature is decreased, the deposition rate increases. However, while the substrate temperature in the initiation or propagation processes is increased, the deposition rate increases, also. The substrate temperature is very important parameter for the monomer surface concentration. At the same time monomer surface

concentration can be related to the ratio of the partial pressure of the monomer, P_M, and the saturation pressure of monomer, P_{sat}. This relation can be explained by the Brunauer-Emmett-Teller or BET adsorption equation in below:

$$\frac{P_M V_m c}{V(P_{sat} - P_M)} = \frac{P_M(c-1)}{P_{sat}} + 1 \tag{1.21}$$

Where V is the volume of monomer that is adsorbed on the substrate and V_m is the volume of a monolayer of monomer, and c is defined as the following equation:

$$c = exp\left(\frac{\Delta H_{des} - \Delta H_{vap}}{RT}\right) \tag{1.22}$$

where R is the gas constant, T is defined as the temperature, ΔH_{vap} is described as the enthalpy of vaporization of the monomer, and ΔH_{des} is also defined as the enthalpy of desorption of a monolayer of monomer from the substrate. At fixed temperature of a gas-liquid system the enthalpy of vaporization, ΔH_{vap}, relates the vapor pressure and boiling point and also the enthalpy of desorption, ΔH_{des}, depends on the monomer and substrate characteristic properties such as polarity, non-polarity of the monomer or hydrophobicity and non-hydrophobicity of the substrate. This c value is generally kept as a constant. The ratio of the partial pressures, P_M/P_{sat} is derived from the BET equation in Eq. 1.21. The deposition rate and molecular weight of the polymers are directly proportional to P_M. Based on the ratio of the partial pressures, P_M/P_{sat}, the BET equation can be reformed in following equation:

$$V = \frac{V_m c \left({}^{P_M}/_{P_{sat}}\right)}{\left(1 - {}^{P_M}/_{P_{sat}}\right)\left[1 - (1-c)\left({}^{P_M}/_{P_{sat}}\right)\right]} \tag{1.23}$$

In ideal situation the volume of adsorbed monomers is close to the monolayer. If the partial pressure of monomer is close to the saturation pressure of monomer, that is, the ratio P_M/P_{sat} approaches to 1, the monomer condenses, so the liquid forms on the surface of the substrate and the conformity decreases. This situation is undesirable, so the condensation should be prevented.

In iCVD system the thermal budget of the process is low, temperatures are close to room temperature, therefore, functional groups of the monomers can stay intact after the process is completed. The iCVD system provides more flexibility because heat sensitive materials such as plastics, especially polymers, pharmaceutics and fabrics etc. can be used due to the lower substrate temperature. (Spee & Rath et al., 2013). There are many applications that iCVD process is used because of due to its advantages. For instances, iCVD process is applied for biological protection, antimicrobial coating, drag delivery, micro-electronics, microfluidics, protective and decorative coating, encapsulation and optical coating.

One of the iCVD applications is antimicrobial coating. Generally, antimicrobial surfaces are used for the textile, fabric and biowarfare protection etc. Antimicrobial agents which provide antimicrobial property are silver based polymers, hydantoin compounds, and phosphonium or quaternary ammonium polymers. However, antimicrobial agents have some problems because they leak from the surface and health, safety and also environmental challenges emerges. Therefore, iCVD process provides a way to solve this problem. The antimicrobial polymers are deposited on the surfaces by applying non-leaching treatment which is the iCVD system because antimicrobial polymers are attached to surface. The deposited thin antimicrobial film can be tested whether the bacterium kills or not. T.P. Martin, S.E. Kooi et al. studied the iCVD of antimicrobial polymer coatings. In that study, poly (dimethyl amino methyl styrene) (PDMAMS) was used as an antimicrobial polymer to provide its antimicrobial properties. The temperature of the filament was set to 604 K by using DC power source. To provide adsorption the substrate temperature was adjusted at 316 K by using recirculating chiller. The reaction pressure was adjusted as 200 mTorr and a fabric which comprised of the nylon shell was used as a substrate. The monomer and the initiator which were a (dimethyl amino methyl) styrene (DMAMS) and di-tert-amylperoxide (TAP), respectively. DMAMS and TAP were vaporized at 343 K and room temperature, respectively. The flow rate of the monomer was adjusted as 2 sccm and the flow rate of the initiator was adjusted as 0.6 sccm. The coating of 120 mg/cm^2 nylon fabric was found to be resistant against to the growth of bacteria effectively 99.9999%. The iCVD technique was an ideal for this kind of application because it does not contain any solvent. It was carried out at the low substrate temperature and the properties of the substrate such as color was not affected. Because of this reasons, this technique can be applied for medical devices (Martin & Kooi et al., 2007).

iCVD polymers have been also used in drug delivery system. Nowadays, the drug delivery technologies have improved quality of human health. During the production of therapeutic drugs, efficiency of these drugs is evaluated based on their absorption rates and kinetics. S. J. McInnes and E. J. Szili et al. studied that a pH responsive drug delivery system which was produced using porous silicon (pSi) by iCVD. The reasons of pSi used was that pSi is known as biodegradable, nontoxic and biocompatible. pSi was loaded with the drugs and a covering layer on pSi was required to protect the drug from detrimental effects in environment. In this study, the filament and the substrate temperatures of iCVD process were adjusted as 285°C and 20°C, respectively. Methyl methacrylate (MAA), ethylene dimethacrylate (EDMA) and tert-butyl peroxide (TBPO) were used as a monomer, cross-linking monomer, and initiator, respectively. Flow rates of MAA, EDMA and TBPO were adjusted as 0.6, 0.1, and 0.1 sccm, respectively. The total reaction pressure was 0.5 Torr in the reactor chamber. After deposition, approximately 350 nm thick p(MMA-co-EDMA) copolymer thin film which showed the pH responsive property at low and high pH. At pH 1.8 drug release rate was slower than at pH 7.4 due to cross-linked film. Drug reached to specific targeting site by using the coated pSi (McInnes & Szili et al., 2012).

iCVD process is also used in microfluidic device fabrication. The microfluidic systems generally contains iCVD compatible polymeric materials such as poly(dimethylsiloxane) (PDMS), polystyrene (PS), poly(methyl methacrylate) (PMMA), poly(ethylene glycol) (PEG), and cyclo-olefin copolymers (COC). Sung Gap Im and Ki Wan Bong et al. reported that by using iCVD process a conformal nano adhesive layer for microfluidic devices were obtained. In this study, in iCVD process glycidyl methacrylate (GMA) was used as a monomer and tert-butyl peroxide (TBPO) was used as an initiator. The flow rates of GMA and TBPO were adjusted as 2.95 sccm and 1.75 sccm, respectively. The pressure of iCVD chamber was set at 200 mTorr. As a result of the deposition, nano adhesive layer of PGMA was thin enough to prohibit clogging of the channels and delimitate the infiltration of the nano adhesive layer into the microfluidic channels (Im & Bong et al., 2009).

One of the most important iCVD application is encapsulation for 3D substrates or liquids. The encapsulation process includes the polymeric materials and liquid environment. There are many techniques which are used for encapsulation. However, these techniques contain solvent(s). The result of the encapsulation process, a wet polymer capsule can be obtained, so the drying is required to evaporate the solvent yet

the aggregation and precipitation of the polymer can occur due to drying. Moreover, the polymer stabilization and the desired coating thickness can be unachievable (Lau & Gleason et al., 2007). Against the all problems, iCVD provides a better solution. For example, Laura C. Bradley and Malancha Gupta studied about ionic liquids (ILs) encapsulation by applying iCVD process. The selection reason of the ILs for encapsulation was that ILs have some useful properties such as being environmentally friendly, nonvolatile, nonflammable and providing toxic gas absorption. IL droplets were encapsulated with the polymers including insoluble fluoropolymers and cross-linked polymers by using iCVD process. In this study, before applying iCVD process, ILs droplets were converted to the liquid marbles by rolling, so polytetrafluoroethylene (PTFE) particles were used to form marbles. After this, IL marbles which was completely coated with PTFE were placed into the iCVD reaction chamber. In iCVD chamber, three different layers which were poly (perfluorodecyl acrylate) (PPFDA), poly (ethylene glycol diacrylate) (PEGDA), and PFDA cross-linked with EGDA (P(PFDA-co-EGDA)) obtained on the IL marbles. Therefore, perfluorodecyl acrylate (PFDA) and ethylene glycol diacrylate (EGDA) were used as monomers and tert-butyl peroxide (TBPO) was used as an initiator. The filament temperature was set at approximately 250˚C. The TBPO initiator, PFDA and EGDA monomers temperatures were regulated at room temperature, 50 and 35 °C, respectively. The flow rate of initiator was adjusted as 1.35 sccm. The cooler temperature was also set as 30 ˚C to provide adsorption. Two different reactor pressures as 80 mTorr and 60 mTorr were for PEGDA and P(PFDA-co-EGDA) depositions and for PPFDA deposition, respectively (Bradley & Gupta et al., 2012).

iCVD technique can be beneficial for various applications providing complex and conformal coatings at low thermal budget and environmentally friendly solventless process. In this study, iCVD method was used for fabrication of protective polymeric coatings on optical surfaces. For this application, surface hydrophobicity and film durability are required for protection from elements such as sudden temperature changes, dust, impact, fog, humidity vibration, radiation so on.

CHAPTER 2

EXPERIMENTAL WORK

In this chapter, details related to materials and iCVD deposition system are given. In addition, entire fabrication procedure is also explained in details.

2.1. Materials

In this study, protective polymeric thin films were fabricated on different substrate materials via iCVD method using selected monomers (with refractive indices between 1.3 and 1.7) and initiator. The protective nano-coatings for optical materials makes economic sense since these materials have high manufacturing and maintenance costs. Therefore, the optical surfaces which are used in many industries and applications should be protected from elements such as sudden temperature changes, humidity, dust, fog, radiation, vibration and impact. To improve the service life, to lower maintenance cost of the systems and to enhance the physical and chemical properties of optical surfaces, polymeric protective nano-coatings can be applied.

Polymeric thin films were obtained as a result of free radical polymerization as previously mentioned. Generally, fluorocarbons, organosilicons, styrenes, acrylates and methacrylates are suitable for coating process because of their properties. The monomers used in this study were Glycidyl Methacrylate (GMA) (97%), Cyclo Hexyl Methacrylate (CHMA) (≥97%), and 1H, 1H, 2H, 2H,-Perfluorodecyl Acrylate (PFDA) (97%). Tert Butyl Peroxide (TBPO) (98%) was used as an initiator. These monomers and initiator were supplied by Sigma Aldrich. Ammonium Hydroxide (NH_4OH) (27%) and Hydrogen Peroxide (H_2O_2) (30%) were used as cleaning chemicals. These chemicals were purchased from Merck Company. The cleaning procedures for substrates are explained in another section. The monomers, initiator, cleaning chemicals and their characteristic properties were listed following Table 2.1.

Table 2.1. Properties of materials used in cleaning process and experiment

Chemicals	Chemical Formula	Molecular Weight (g/mol)	Boiling Point	Flash Point
Glycidyl Methacrylate (GMA)	$C_7H_{10}O_3$	142.15	189 ˚C	76 ˚C
Cyclo Hexyl Methacrylate (CHMA)	$C_{10}H_{16}O_2$	168.2	93.75 ˚C	81 ˚C
1H,1H,2H,2H,-Perfluorodecyl Acrylate (PFDA)	$C_{13}H_7F_{17}O_2$	518.17	90 ˚C	113 ˚C
Tert Butyl Peroxide (TBPO)	$(CH_3)_3COOC(CH_3)_3$	146.23	110 ˚C	1 ˚C
Ammonium Hydroxide	NH_4OH	35.05	37.7 ˚C	-
Hydrogen Peroxide	H_2O_2	34.015	106 ˚C	-

Table 2.2. (Cont.) Properties of materials used in cleaning process and experiment

Chemicals	Melting Point	Vapor Pressure	Refractive Index	Supplier
Glycidyl Methacrylate (GMA)	-52 ˚C	3.15 mmHg @ 25°C	1.449	Sigma-Aldrich
Cyclo Hexyl Methacrylate (CHMA)	-104 ˚C	0.138 mmHg @ 20°C	1.4578	Sigma-Aldrich
1H,1H,2H,2H,-Perfluorodecyl acrylate (PFDA)	-4 ˚C	-	1.337	Sigma-Aldrich
Tert Butyl Peroxide (TBPO)	-40 ˚C	40 mmHg @ 20 °C	1.3891	Sigma-Aldrich
Ammonium Hydroxide	-57.5 ˚C	362.28 mmHg @ 20 °C	-	Merck
Hydrogen Peroxide	-26 ˚C	13.5 mmHg @ 20 °C	-	Merck

2.1.1. Cleaning Procedures for Substrates

The substrates to be coated were chosen as crystalline silicon (c-Si) and glass (microscope slide) due to their characteristic features and their relatively low costs. In coating process, cleaning of substrates are a vital issue because any impurities like microscopic particles, dust etc. can potentially have detrimental impact on film properties. To remove organic or other types of contaminants from the c-Si and glass substrates, two different procedures were used for each of them.

For the glass substrate, the cleaning procedure was simple. In this procedure, glasses were cut properly and they were placed into beaker with soapy water at 50 ˚C ultrasonic bath during 30 minutes. Glasses was removed from ultrasonic bath by washing

with deionized water and ultrasonic bath was applied again with deionized water at 50˚C 30 minutes. The cleaned glasses were dried by using vacuum oven at 60˚C for 30 minutes. After the cleaning procedure was performed, glasses were ready for coating. The cleaning procedures were shown in following Figure 2.1.

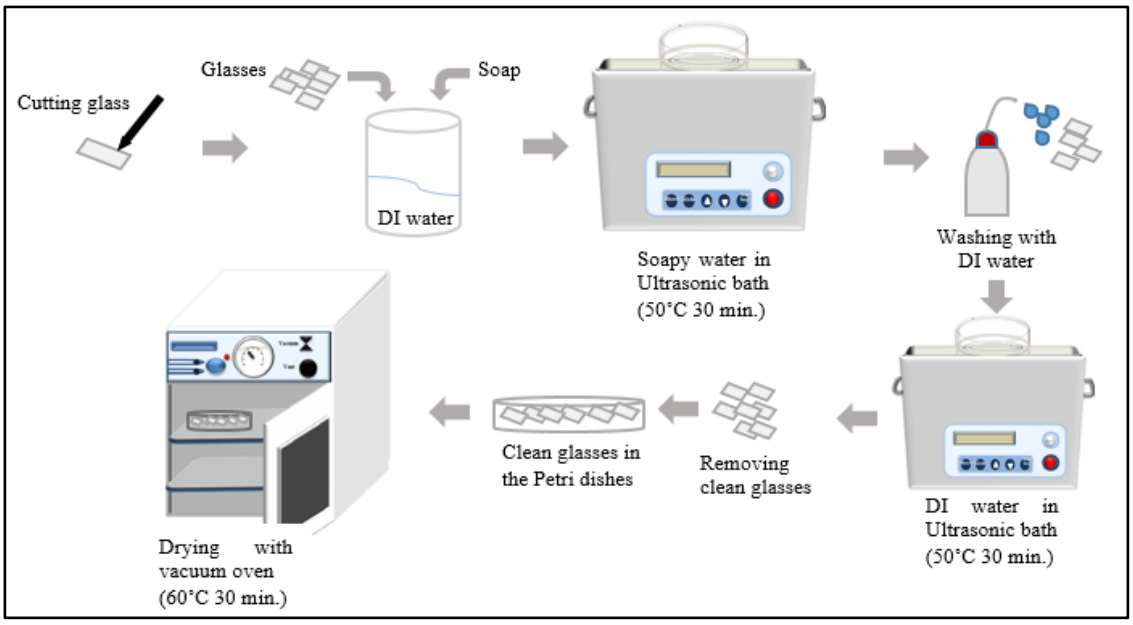

Figure 2.1. The cleaning procedure for glasses

For the c-Si, famous industry standard RCA cleaning procedure are performed to remove organic and ionic contamination. Cleaning procedure for c-Si substrates used in this study contains the following chemical steps performed in sequence:

First, 325 ml deionized water was put into a Pyrex beaker, then 65 ml NH_4OH (27%) was added into this beaker and then this solution was heated up to 70 ˚C on the hotplate. After heating, 65 ml H_2O_2 (30%) was added. When bubbles formed the solution was ready for use in cleaning of the c-Si substrates. Silicon wafers were soaked in the solution for 15 minutes. The wafers were transferred to a container with overflowing DI water to remove the solution. Finally, the wafers were removed from water. To dry these wafers, they were put into vacuum oven. These wafers were ready for experiment. The RCA procedure was shown in following Figure 2.2.

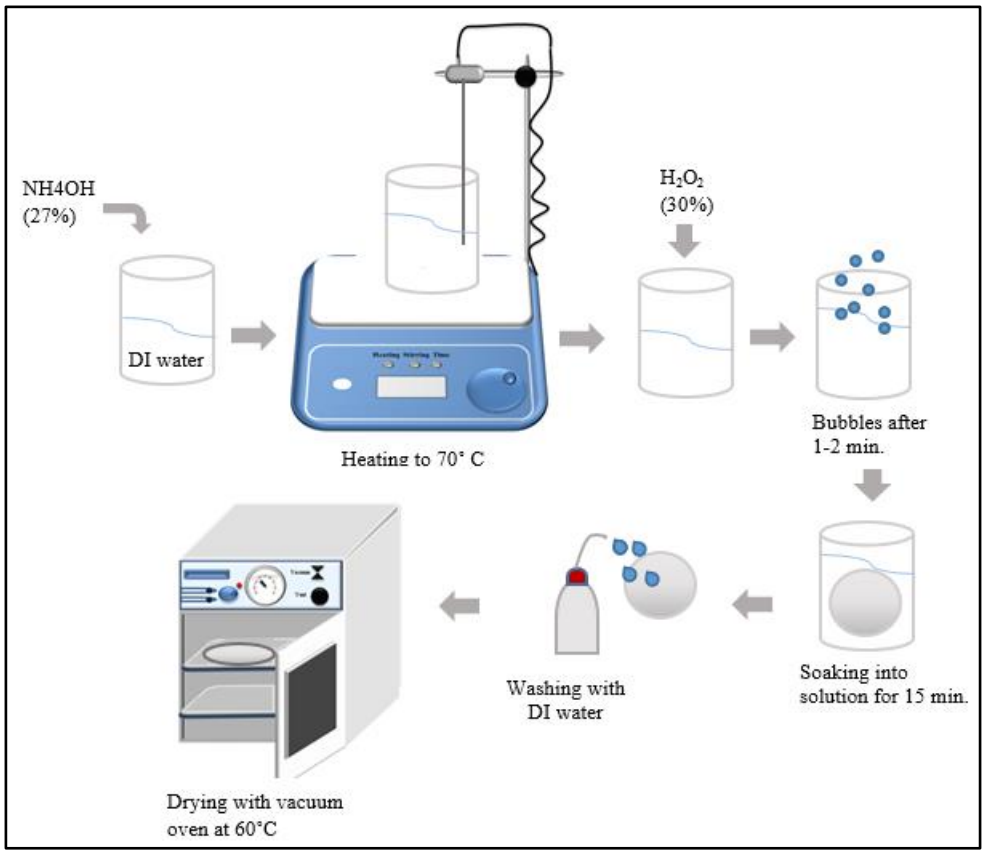

Figure 2.2. The RCA cleaning procedure for silicon wafer

2.2. CVD Experimental Set-Up

Before CVD experimental set-up is explained, general information should be given about iCVD system. In vacuum chamber, free radical polymerization reaction takes place in the presence of initiator and monomer. Thermal activation of initiator is provided by heated filaments. To promote adsorption, the surface to be coated should be kept at a much lower temperature. iCVD system does not require solvent, three dimensional and complex coatings can be provided (Lau & Gleason et al., 2006).

In iCVD system, the shape of reactor geometry was shown in Figure 2.3. The reactor was square-shaped with a height of 4 cm and length of 31.6 cm. The reactor was equipped with filament arrays spaced approximately 1.5 cm apart and also suspended over the surface of the substrate at a distance of 2.9 cm. These filaments were Nichrome filaments (80% Ni/20% Cr, Omega Engineering) which were resistant to heat. They provided thermal energy for decomposition of chemicals. Generally, they were heated up to 350 ˚C and the temperature was measured by a thermocouple (Type K, Omega Engineering) attached to one of the filaments directly. The substrate temperature was

controlled by a recirculating chiller/heater (WiseCircu). The circular shaped backside-cooled stage was 24 cm in diameter.

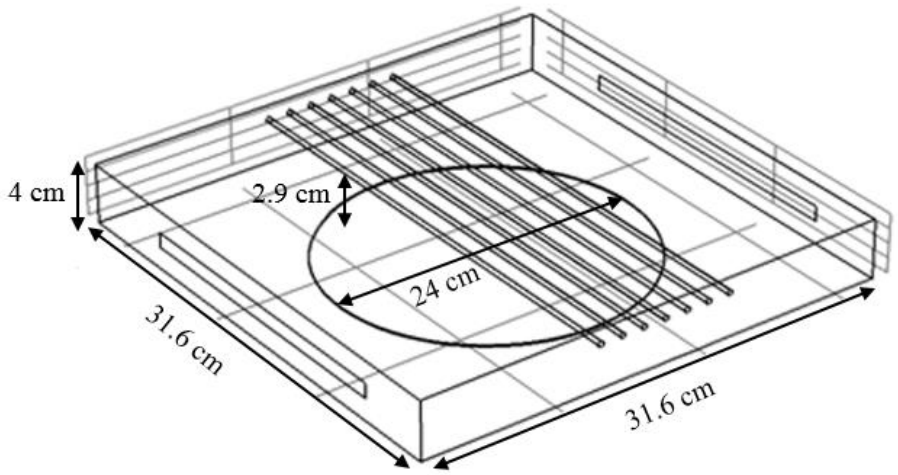

Figure 2.3. CVD reactor geometry

A removable quartz plate (12.5 cm radius and 2.5 cm thick) was used as the top plate of the reactor, so substrate could be observed in the reactor chamber. Time was recorded during deposition to determine deposition rate. During deposition, precursors were introduced from inlet port which was located at the right side of the reactor. After polymerization reaction, the gases left the chamber from opposite end of the reactor. Reactor pressure was controlled with a throttling butterfly valve (Model 253B, MKS Type). Precursors were delivered into a vacuum chamber which was maintained at a pressure between 10^{-1} and 1 Torr. Vacuum was attained by a pump (2XZ-Rotary Vacuum Pump). Monomer and initiator flow rates were controlled by mass flow controllers (MFCs). Monomers and initiator were transferred into the reaction chamber by using MFCs channels which were MFC1 (MKS type 1479A), MFC2 (MKS type 1150C) and MFC3 (MKS type 1479A). MFC1, MFC2, and MFC3 had different capacities because the flow rates of monomers and initiator were not the same. These capacities were 20 standard cubic centimeters per minute (sccm), 10 sccm and 100 sccm, respectively. Generally, MFC1 and MFC3 were used for monomer and initiator which had high vapor pressure, so they were vaporized easily. The temperatures of chemical containers, lines and reactor were controlled with Proportional Integral Derivatives (PIDs) controllers (Omega Engineering).

2.3. Thin Film Deposition

In these study, PGMA (poly glycidyl methacrylate), PCHMA (poly cyclohexyl methacrylate), PPFDA (poly perfluorodecyl acrylate), P (GMA-PFDA) (poly glycidyl methacrylate and poly perfluorodecyl acrylate) copolymer thin film deposition were performed by changing of the reaction pressure, mass flow rates, and temperatures.

PGMA Thin Film Deposition:

Before starting the experiment, mass flow controllers (MFCs) calibration was carried out for GMA and tert-butyl peroxide (TBPO) because all mass flow controllers were factory calibrated with nitrogen. The reactor volume was determined as approximately 5.57 liters. During calibration, the changing of pressure was recorded for a fixed time period. The calibration graphs of GMA and TBPO were shown in Appendix A. There are many parameters which affect the film properties. Before the experimental parameters were selected, a detailed literature survey was conducted. Flow rates of GMA and TBPO were used as 1.5 ccm and 1 ccm, respectively. The substrate temperature was kept constant as 35˚C and the filament temperature was set as 330˚C. Additionally, total pressure was adjusted as 500 mTorr. As a result, the deposition rate was found as approximately 15 nm/min. GMA was attached to MFC2 and it was heated to approximately 60-65 ˚C to provide desired mass flow. The initiator, TBPO, was vaporized at room temperature. To avoid condensation, all flow lines in iCVD system was heated to 80 ˚C. To investigate the effects of total pressure on the thin films thicknesses, all parameters were kept constant and total pressure was changed gradually. The other parameters values, which were selected according to the literature, were given as Table 2.2.

PCHMA Thin Film Deposition:

CHMA and TBPO were attached to MFC2 and MFC3, respectively. Calibration was done with MFC2 for CHMA. The flow rates of CHMA was defined in calibration graph which is given in Appendix A. CHMA was heated to 65 ˚C. The experimental parameters were again chosen from literature. The mass flow rates of CHMA and TBPO

were kept constant as 1.5 ccm and 1 ccm, respectively. At the same time, the filament temperature was adjusted as 330˚C and the substrate temperature was kept constant as 35˚C and total pressure was used as 500 mTorr. To obtain a good PCHMA thin film on c-Si, the total pressure was 300 mTorr and deposition time was determined as 50 minutes. Other parameters were shown in Table 2.2.

PPFDA Thin Film Deposition:

Fluoropolymer coatings which are used in many applications such as modern industrial, household and construction products. Coatings which involves fluoro chemicals are applied in anti -reflection coatings, antifouling coatings for eyeglass lenses and protective coatings for exterior substrate. Fluorine atoms have high electronegativity and low polarizability. Perfluoropolymers which contain C-F bonds were used for this study. Perfluoropolymers have excellent weather resistance because there is the small dipole moment, which provides to oil-water repellency, low surface tension, low refractive index, reduced adhesion to surfaces and also low friction (Jones, 2008). 1H, 1H, 2H, 2H,-Perfluorodecyl acrylate (PFDA) was used as monomer to obtain PPFDA thin film. In this experiment, PFDA and TBPO were used at MFC2 and MFC1, respectively. The temperature of PFDA was adjusted as 85˚C because of its low vapor pressure. The calibration graphs of PFDA and TBPO were shown in Appendix A. Flow rates of PFDA and TBPO were adjusted as 0.42 ccm and 0.82 ccm, respectively. The total pressure was set as 100 mTorr. Temperatures of substrate and filament were 44 ˚C and 300 ˚C, respectively. The deposition rate was found as 150 nm/min. Additionally, temperatures of the filament and substrate were set as 250 ˚C and 35 ˚C, respectively. The parameters of this study were given in Table 2.2.

P (GMA-PFDA) Thin Film Deposition:

In order to fabricate thin films which have both of good mechanical properties and super hydrophobic surface, copolymer thin films was performed in iCVD system by using GMA and PFDA as monomers. The mechanical properties of fluorinated acrylate materials are poor because of their chemical structure. Therefore, copolymerization have been carried out to improve the performance of fluoropolymers. GMA, which has the strong mechanical properties, and PFDA, which was also known as fluorinated acrylate,

were used as monomers. For copolymer thin film experiment, the manual mass flow controller (MMFC) was added to the iCVD system for GMA monomer. Calibration of GMA was done with MMFC. PFDA monomer was used with MFC2 and TBPO was used with both MFC1 and MFC3, for different experiments. Therefore, the previous calibration graphs of TBPO and PFDA were used, and GMA which was calibrated with MMFC is shown in Appendix A. The flow rates of monomers and initiator and the other parameters were selected based on a literature study (Paxson & Yagüe et al., 2014). The filament and substrate temperatures were set as 300 ˚C and 35 ˚C, respectively. The other experimental parameters which are shown as Table 2.2.

Table 2.3. The experimental parameters for thin film deposition

Run No	**Monomer**	**Initiator**	**$F_{monomer}$ (ccm)**	**$F_{initiator}$ (ccm)**	**$T_{filament}$ (˚C)**	**$T_{substrate}$ (˚C)**	**P_{total} (mTorr)**	**Time (min)**
1	GMA	TBPO	1.5	1	330	35	250	30
2	GMA	TBPO	1.5	1	330	35	300	30
3	GMA	TBPO	1.5	1	330	35	350	30
4	GMA	TBPO	1.5	1	330	35	400	30
5	GMA	TBPO	1.5	1	330	35	450	30
6	GMA	TBPO	1.5	1	330	35	500	30
7	GMA	TBPO	3.5	1	330	35	500	20
8	GMA	TBPO	1.5	1	330	35	250	30
9	GMA	TBPO	1.5	1	330	35	500	45
10	CHMA	TBPO	1.5	1	330	35	500	50
11	PFDA	TBPO	0.42	0.15	250	35	75	15
12	PFDA	TBPO	0.42	0.15	250	35	50	20
13	GMA-co-PFDA	TBPO	0.3-0.3	0.3	300	35	80	20
14	GMA-co-PFDA	TBPO	0.418-0.44	1.2	300	35	200	7.5

2.4. Characterization

The thickness of polymer films deposited was measured with SemiconSoft, Inc. instrument shown in Figure 2.4. With this system, any translucent material which is in 15nm-50 μm thickness range can be measured rapidly between 400-1000 nm ranges.

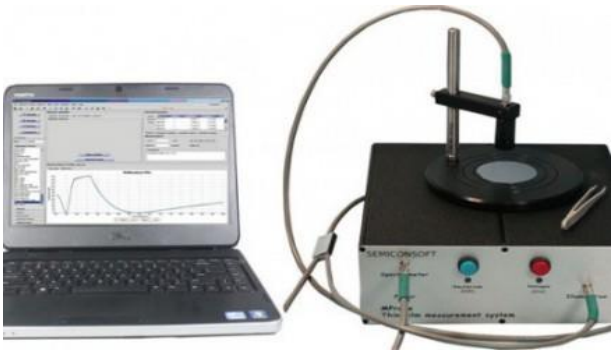

Figure 2.4. The SemiconSoft, Inc. measurement instrument
(Source: SemiconSoft 2013)

Perkin Elmer FTIR System Spectrum BX equipment was used for chemical analysis of deposited polymeric films. The morphology of polymeric thin films was investigated with Scanning Electron Microscopy (SEM) (FEI Quanta250). When necessary a thin conducting film was sputtered before SEM analysis. The surface roughness of the polymeric thin film was determined with Atomic Force Microscopy (AFM). A Nanosurf Flex-ANA system was used in tapping mode. Nanosurf software was used for roughness calculation and image processing. Theta Lite contact angle measurement was used to determine the wettability of the surface.

CHAPTER 3

RESULTS AND DISCUSSION

In this chapter, results of deposition experiments which include PGMA, PCHMA, PPFDA and a copolymer P(GMA-PFDA) film coatings obtained using iCVD method are given.

3.1. Fabrication of PGMA, PCHMA, PPFDA and P(GMA-PFDA) Thin Films

The deposition procedure, which was explained in Chapter 2, is nearly the same for all coating materials. However, the deposition conditions and experimental parameters of the materials are different from each other. Therefore, in this study for all PGMA, PCHMA PPFDA and copolymer film depositions, operating conditions were varied to obtain the desired film thicknesses. As a result of deposition experiments, thin film thicknesses and deposition rates are shown in Table 3.1 in detailed.

Table 3.1. The results of thin film deposition experiments

Run No	Monomer	Initiator	Time (min)	Thickness (nm)	Deposition rate (nm/min)
1	GMA	TBPO	30	389±78	~13
2	GMA	TBPO	30	419±39	~14
3	GMA	TBPO	30	638±7	~21.3
4	GMA	TBPO	30	676±60	~22.5
5	GMA	TBPO	30	732±19	~24.4
6	GMA	TBPO	30	752±61	~25.1
7	GMA	TBPO	20	1430±40	~71.5
8	GMA	TBPO	30	367±50	~12.2
9	GMA	TBPO	45	1000±20	~22.2
10	CHMA	TBPO	50	975±25	~19.5
11	PFDA	TBPO	15	390±30	~26
12	PFDA	TBPO	20	181±24	~9
13	GMA-co-PFDA	TBPO	20	~1000	~50
14	GMA-co-PFDA	TBPO	7.5	656±14	~87

PGMA thin film thicknesses increased with increasing reactor pressure because a greater amount of GMA and TBPO passed through MFCs proportionally their mass flow rates. At the same time, deposition rate was calculated using thin film thickness and deposition time. Therefore, the desired thin film thicknesses can be obtained by adjusting deposition time. When the thickness measurement was carried out by using reflectometry which is the SemiconSoft, Inc. measurement instrument, reflectance versus wavelength graphs were created based on the coated polymer properties. Thin film thicknesses were determined by comparing measured and calculated reflectance data in these graphs.

When the result of 10^{th} experiment was investigated on Table 3.1, PCHMA thin film thickness was measured as 975 nm with reflectometry. PPFDA thin film deposition was carried out by using the selected experimental parameters, the results of 11^{th} and 12^{th} experiments, PPFDA thin film thicknesses were found as 390 nm and 181 nm by using reflectometry, respectively. To observe the effects of flow rates and the total pressure, two copolymer thin film experiments were carried out. As results of 13^{th} and 14^{th} experiments, the thicknesses of thin films were found approximately 1000 nm and 656 nm, respectively. At 14^{th} experiment deposition time was kept as 7.5 min, so thin film thickness was found lower than the previous experiment even if the total pressure and the flow rates of monomer and initiator were higher.

3.2. SEM Analysis of Thin Films

In order to investigate film morphology and surface uniformity of coated films on c-Si substrate in iCVD system, SEM was performed for all thin films.

3.2.1. SEM Analysis of PGMA Thin Films

When the 4^{th} experiment was investigated, thin film thickness was found as 676 nm by using reflectometry as seen on Table 2.2. At the same time, to analyze surface and to control thin film thickness which was PGMA, SEM characterization was performed on the coated substrate. Before deposition, a portion of the substrate was covered with a tape. After deposition, the tape was removed from surface and thickness of the film was also measured in SEM. SEM images were shown below with Figure 3.1.

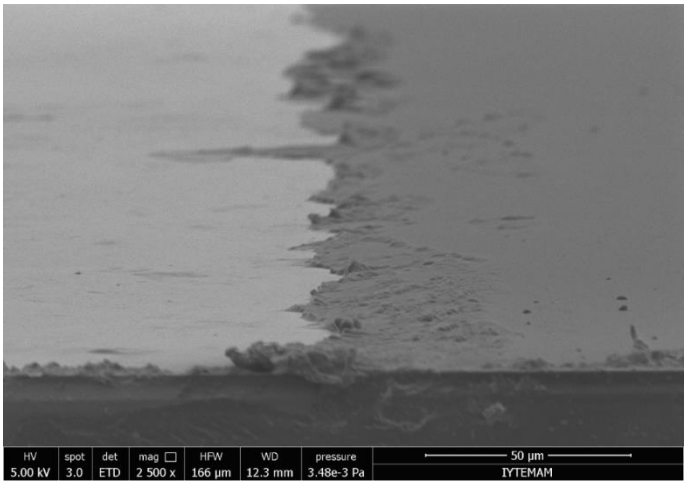

Figure 3.1. SEM images of PGMA thin film on c-Si substrate

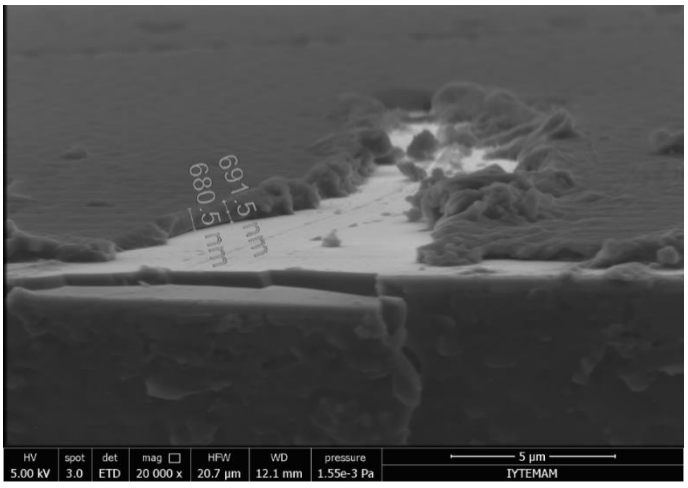

Figure 3.2. SEM images of the cross sectional areas of PGMA thin film on c-Si

As shown above Figure 3.1 and Figure 3.2, the surfaces were characterized by SEM at 50 µm and 5 µm scales, respectively. As seen in the first SEM image, after removing tape from the silicon wafer, it was observed that PGMA was not coated on the left side and the right side of silicon wafer coated properly with PGMA and thin film thickness was measured as approximately between 680 and 691.5 nm looking at cross sectional area of thin film. When the reflectometry measurement and SEM images of PGMA thin film thickness were compared, they were nearly the same. The surfaces of uncoated c-Si and ~1 µm PGMA film which was obtained as a result of 9th experiment were shown in Figure 3.3 and Figure 3.4.

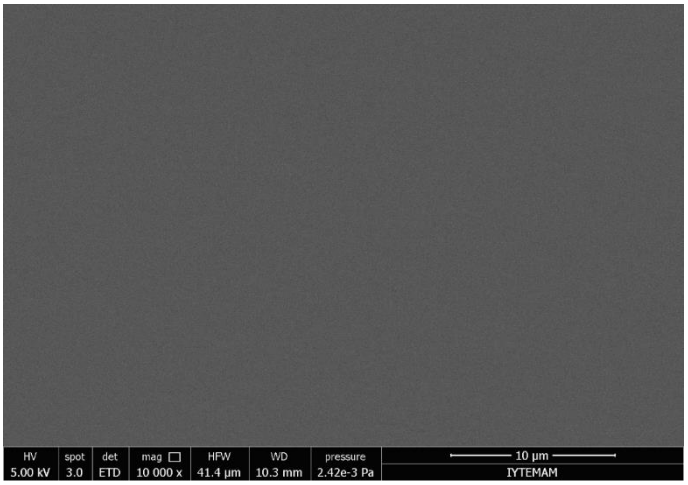

Figure 3.3. SEM image of the surface of uncoated c-Si substrate

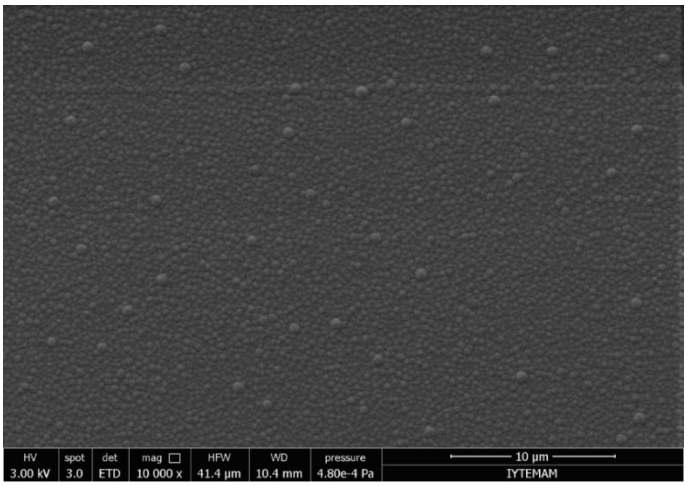

Figure 3.4. SEM image of the surface of ~1µm PGMA thin film on c-Si

Figure 3.3 and Figure 3.4 showed that SEM images were taken at 10µm scale. When the surface of uncoated and coated substrate with ~1µm PGMA thin film were investigated, it was observed that ~1µm PGMA thin film covered entire substrate surface without any visible defects. Similar bead like PGMA film morphology was also reported in literature (Mao and Gleason, 2004).

3.2.2. SEM Analysis of PCHMA Thin Films

To investigate the surface of PCHMA thin film on c-Si substrate, SEM images were taken at different magnifications. These SEM images with 10μm and 30 μm scale bars, respectively, were shown in following figures.

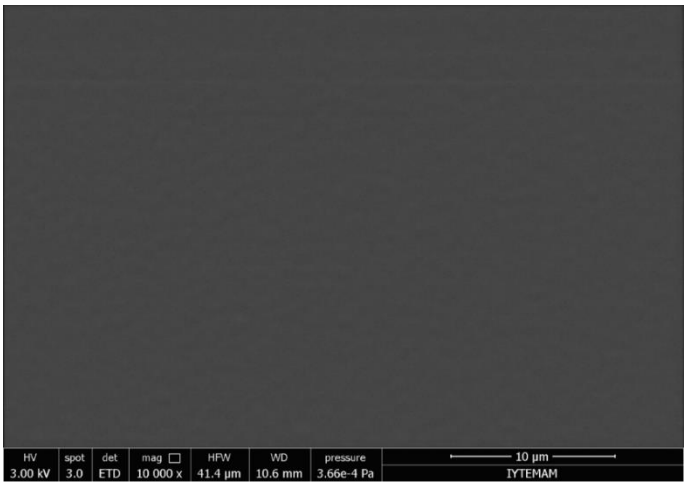

Figure 3.5. SEM image of the PCHMA thin film on c-Si

SEM image revealed that the PCHMA thin film was coated on the c-Si uniformly at the same time, PCHMA thin film was smoother than the PGMA thin film because of their different chemical structures.

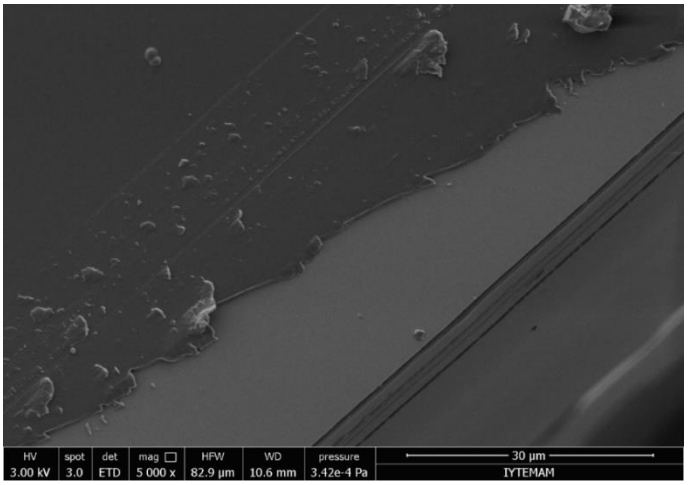

Figure 3.6. SEM image of the edge of PCHMA thin film on c-Si

The edge of PCHMA thin film was investigated with SEM to compare the film thickness with reflectometry measurements. Other than some surface damage, more likely

due to handling of the sample, no significant defect such as pinholes was observed on the sample.

3.2.3. SEM Analysis of PPFDA Thin Films

To compare thin film thicknesses and to evaluate the film morphology, SEM images of PPFDA films were taken at different magnifications.

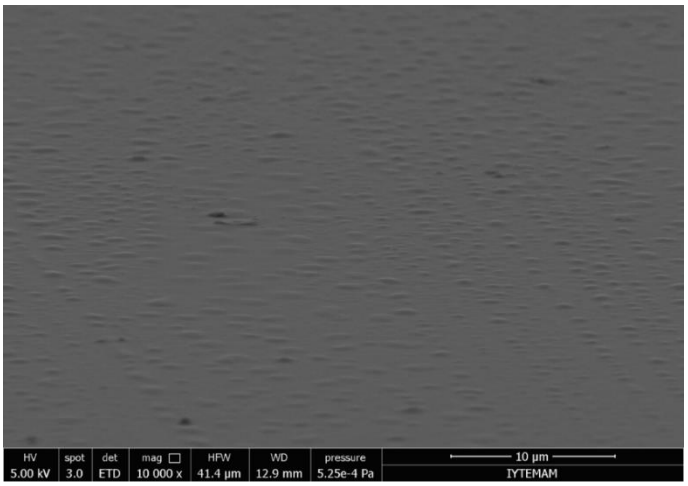

Figure 3.7. SEM image of the surface of PPFDA thin film on c-Si

In Figure 3.7, SEM image showed that polymerization taken place successfully on the surface of the c-Si substrate because PPFDA thin film was coated over the entire substrate surface without any defects such as pinhole and scratches (11th experiment).

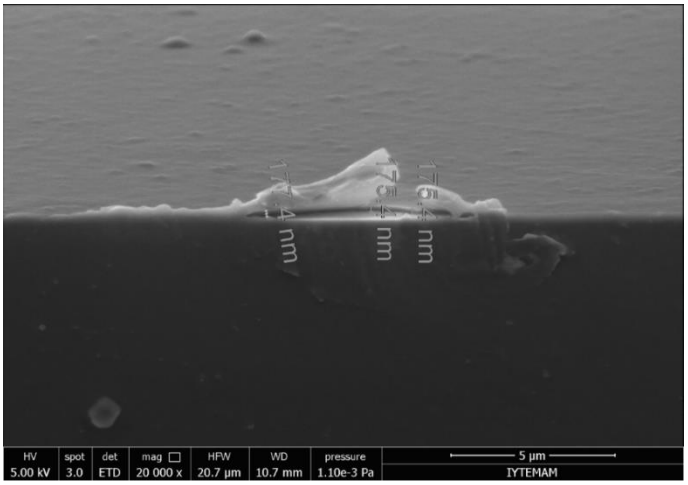

Figure 3.8. SEM image of the cross section of PPFDA thin film on c-Si

As shown in Figure 3.8, the result of the 12th experiment, the cross sectional area of thin film was investigated by SEM at 5 μm scale. Film thickness was measured as 181 nm by reflectometry and also as 175.4 nm by using SEM.

In iCVD system, PPFDA thin film deposition was performed not only on c-Si but also on paper and tissue paper. SEM images of uncoated tissue paper and PPFDA thin film coated on tissue paper were shown in Figure 3.9 and Figure 3.10.

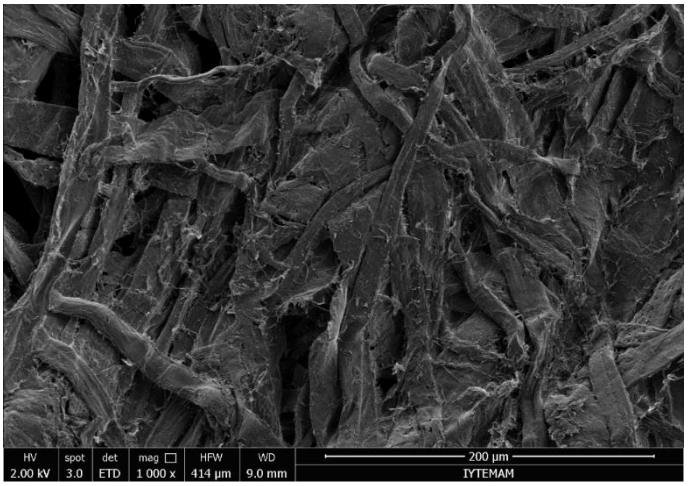

Figure 3.9. SEM image of the surface of uncoated tissue paper

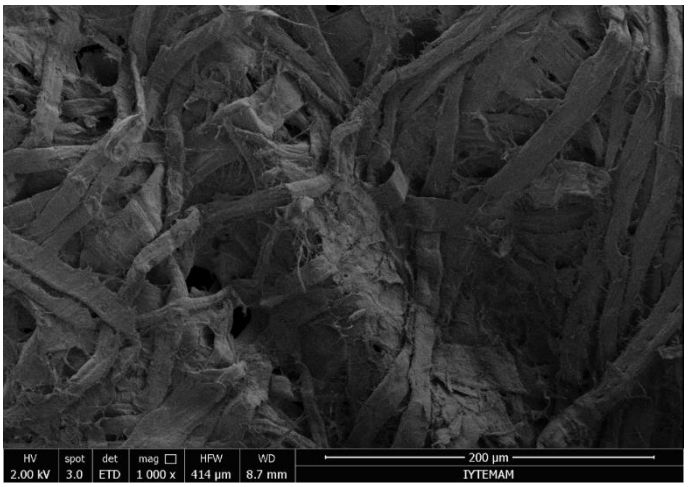

Figure 3.10. SEM image of the surface of PPFDA thin film coated on tissue paper

In Figure 3.9 and Figure 3.10, it was observed that individual fibers in uncoated tissue paper was more evident than the fibers in PPFDA coated tissue paper. The surface of coated tissue paper was smoother than the surface of the uncoated tissue paper as expected.

3.2.4. SEM Analysis of P(GMA-PFDA) Thin Films

To examine the surface and the cross sectional area of these samples, SEM images were taken at different magnifications. The SEM results were demonstrated as seen on figures below.

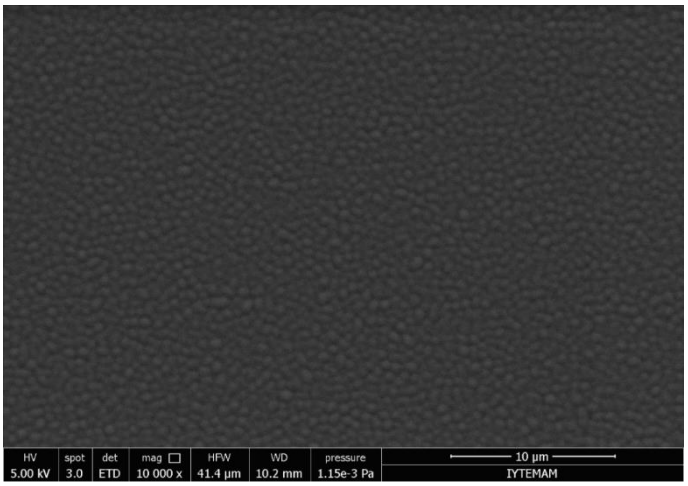

Figure 3.11. SEM image of the surface of ~1000 nm copolymer thin film on c-Si

As seen on Figure 3.11 SEM image was taken at 10µm scale. A continuous copolymer thin film covered the surface entirely. Besides, it was seen that the surface morphology of copolymer coated on c-Si was similar to the surface morphology of PGMA coated on c-Si with bead like structures and relatively rough surface compared to bare c-Si.

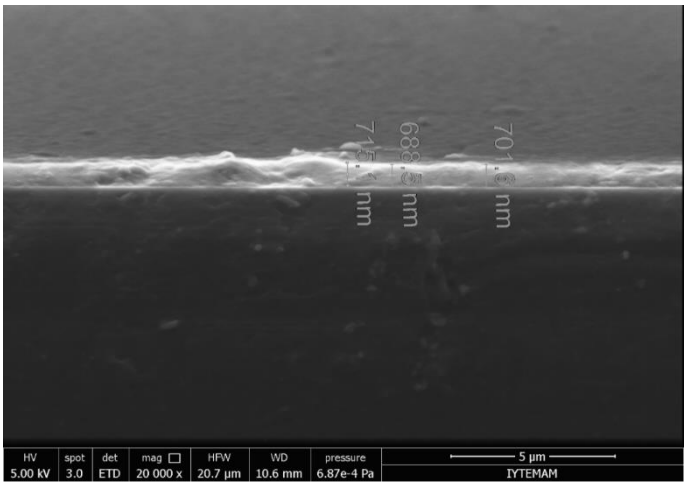

Figure 3.12. SEM image of the cross sectional area of 656 nm copolymer thin film on c-Si

Figure 3.12 showed the film cross section at 5 μm scale. It was seen that the surface of c-Si was coated with copolymer thin film, however, the film thickness was measured from its cross section as 700 nm. The reflectometry result and SEM result were almost same, but the reason for the little difference could have been the edge effects. Some thickness variations were observed at the edges of the sample.

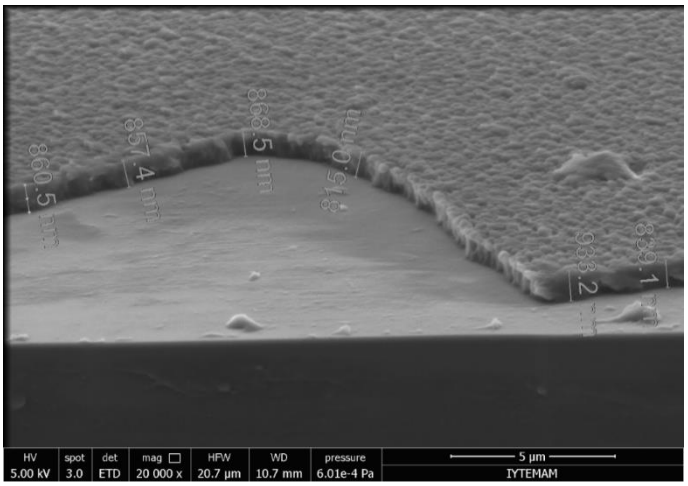

Figure 3.13. SEM image of the cross sectional area of ~1000 nm copolymer thin film on c-Si

As seen on Figure 3.13 copolymer thin film was observed on c-Si. SEM image was taken at 5μm scale and thin film thickness was measured as 871 nm, however, normally thin film thickness was measured as approximately 1000 nm. The reason of this situation was the edge effect and nonuniformity at the edge of the sample thin film.

3.3. FTIR Analysis of Monomers and Thin Films

To evaluate the chemical composition of the polymer films and to investigate whether polymerization was performed efficiently or not, FTIR analysis of monomers and thin films was performed.

3.3.1. FTIR Analysis of GMA Monomer and PGMA Thin Films

PGMA coated on c-Si, and GMA as a monomer were analyzed by FTIR spectroscopy. The aim of characterization of the monomer was to determine whether unreacted monomer was on PGMA thin film or not. If unreacted monomer remained on the PGMA thin film, the results of FTIR would show some specific peaks of monomer. FTIR spectra of monomer and PGMA thin film are given as the following Figure 3.14.

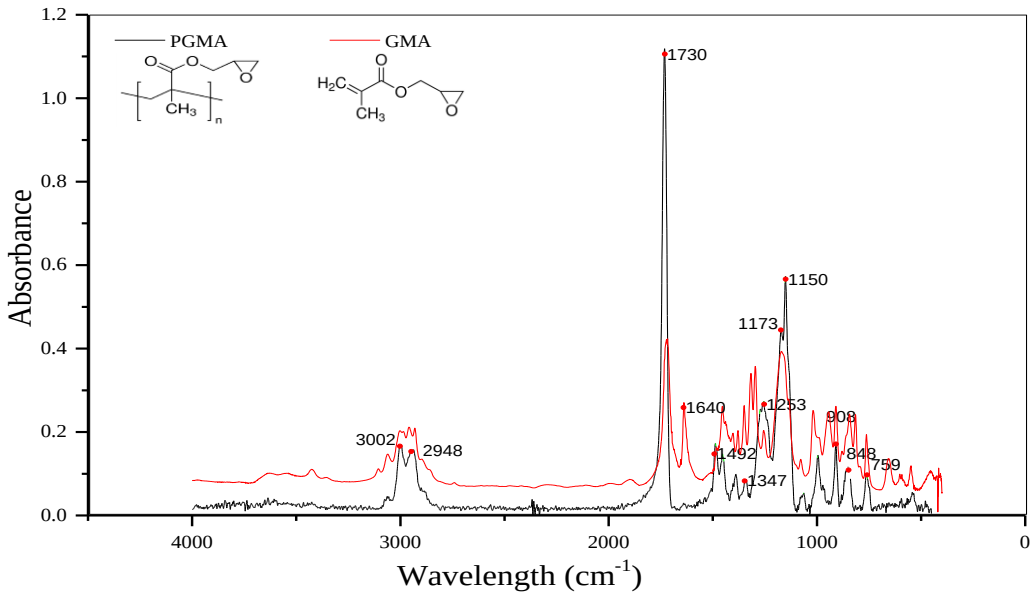

Figure 3.14. FTIR spectra of monomer and polymer form of GMA thin film on c-Si

Both of monomer and polymer results showed some specific peaks. In literature, C–H symmetry and asymmetry stretching peaks are identified at 3000 and 2935 cm^{-1} corresponding to methyl and methylene groups, respectively (Aegerter & Mennig et al., 2004). These C–H symmetry and asymmetry stretching peaks appeared at 3002 and 2948 cm^{-1} for monomer and polymer. The absorption peak which assigned to the carbonyl (C=O) stretching vibration due to the ester group was observed at 1730 cm^{-1}. Besides, in the monomer spectrum, at 1640 cm^{-1} C=C stretching peak was observed clearly, however, in the polymer spectrum this specific peak was absent. Therefore, it was concluded that unreacted monomer did not remain in polymer. Moreover, GMA has epoxide group in its structure, hence, in the FTIR results of monomer and polymer the characteristic absorption bands were obtained at 908, 848 and 759 cm^{-1} for epoxide groups (Gupta &

Gleason et al., 2006; Bakker & Verlaan et al., 2007) proving that the functional groups in monomer are not affected during polymerization.

3.3.2. FTIR Analysis of CHMA Monomer and PCHMA Thin Films

FTIR spectra of CHMA monomer and PCHMA thin film are given below in Figure 3.15.

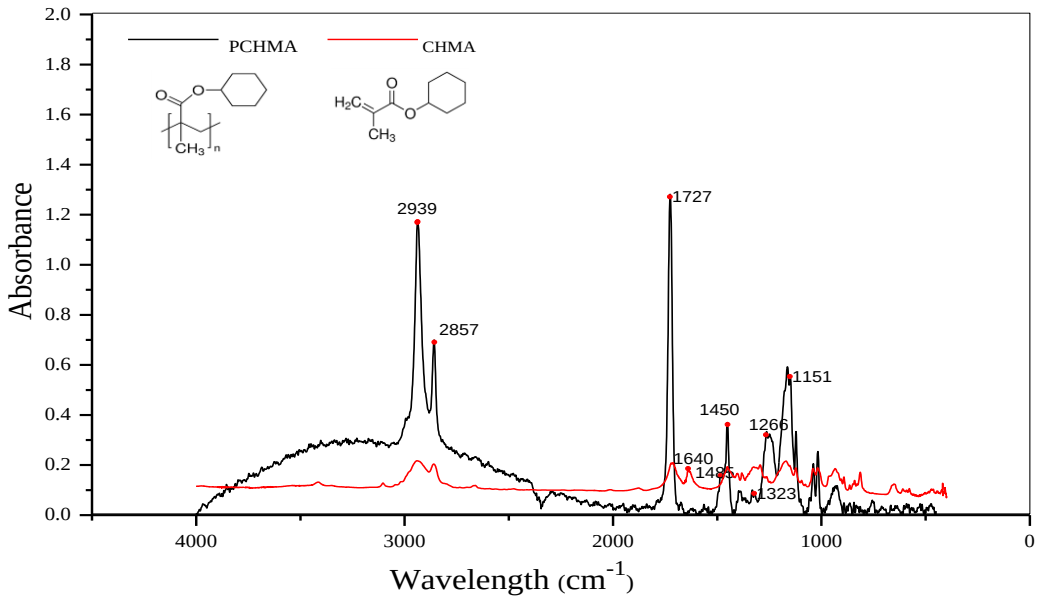

Figure 3.15. FTIR spectra of monomer and polymer form of CHMA thin film on c-Si

Both monomer and polymer form of CHMA showed two specific peaks at 2939 and 2857 cm^{-1} caused by the CH_2 asymmetrical and symmetrical cyclohexyl vibrations respectively (Xu & Gleason et al., 2011). Moreover, the prominent peak at around 1727 cm^{-1} attributed to the C=O stretching and the peak at 1640 cm^{-1} assigned to C=C stretching was not observed in the polymer spectrum in figure above because there was not monomer in the deposited film. However, this specific peak observed clearly in the monomer spectrum. Furthermore, the peaks not specifically but partially observed around 1500-1350 cm^{-1} assigned to C-H bending. The (O=) C-O stretching vibrations bands occurred between 1300 and 1150 cm^{-1} (Xu & Gleason et al., 2011).

3.3.3. FTIR Analysis of PFDA Monomer and PPFDA Thin Films

PPFDA polymer and PFDA monomer were characterized using FTIR. The results of the FTIR spectra analysis of monomer and PPFDA thin film were shown in Figure 3.16.

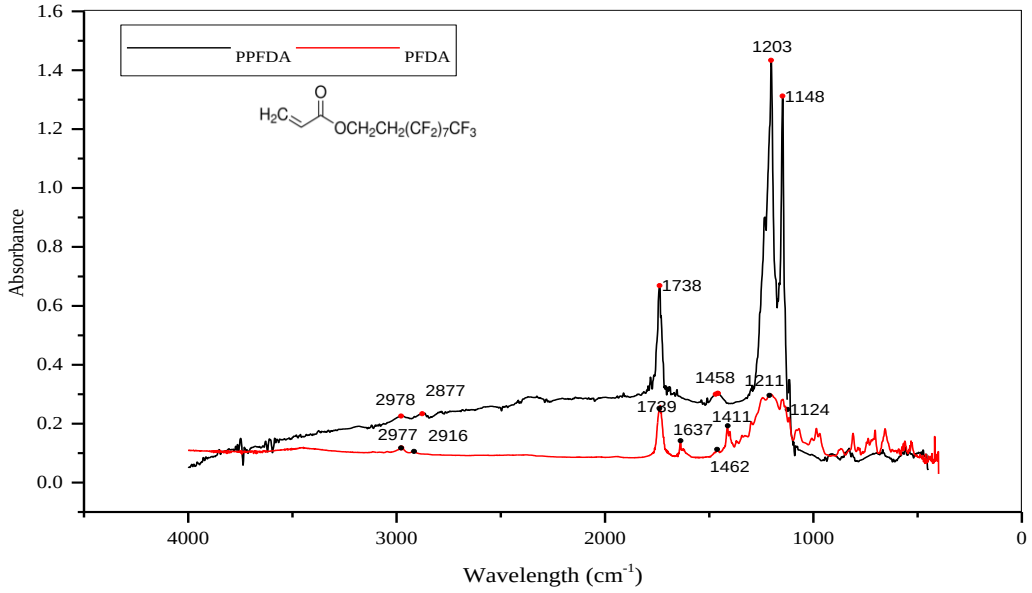

Figure 3.16. FTIR spectra of monomer and polymer form of PFDA thin film on c-Si

Figure 3.16 shows FTIR spectra in the region between 4000 and 400 cm^{-1}. At both spectra, the sharp peak of C=O stretching was at 1738 and 1739 cm^{-1}. At the same time, both the monomer and the polymer spectra contained three strong, sharp absorbance peaks in the 1350-1120 cm^{-1} region. The asymmetric stretching and symmetric stretching of the -CF2- moiety caused the sharp peaks at 1211 and 1207 cm^{-1}, respectively. The sharp peak at 1148 cm^{-1} was caused by the -CF2-CF3 end group. In the FTIR spectra of PPFDA thin film, the narrowness of the peaks showed the chemical homogeneity. The additional peaks at 1637, 1462, 1411 cm^{-1} and some peaks from 1080 to 968 cm^{-1} existed on the monomer spectrum. These peaks were the characteristic absorbance bands for the C=C double bond. PPFDA thin film spectrum did not show these peaks. The polymer and monomer spectrum contained peaks in the regions 2978-2877 cm^{-1}, which were associated with the C-H stretching and CH_2 vibrations on a saturated carbon atom (Gupta & Gleason et al., 2006).

3.3.4. FTIR Analysis of P(GMA-PFDA) Thin Films

Copolymer P(GMA-PFDA) thin film samples were also characterized using FTIR. The results of the FTIR spectrum analysis of two different copolymer thin films were shown as Figure 3.17 and Figure 3.18.

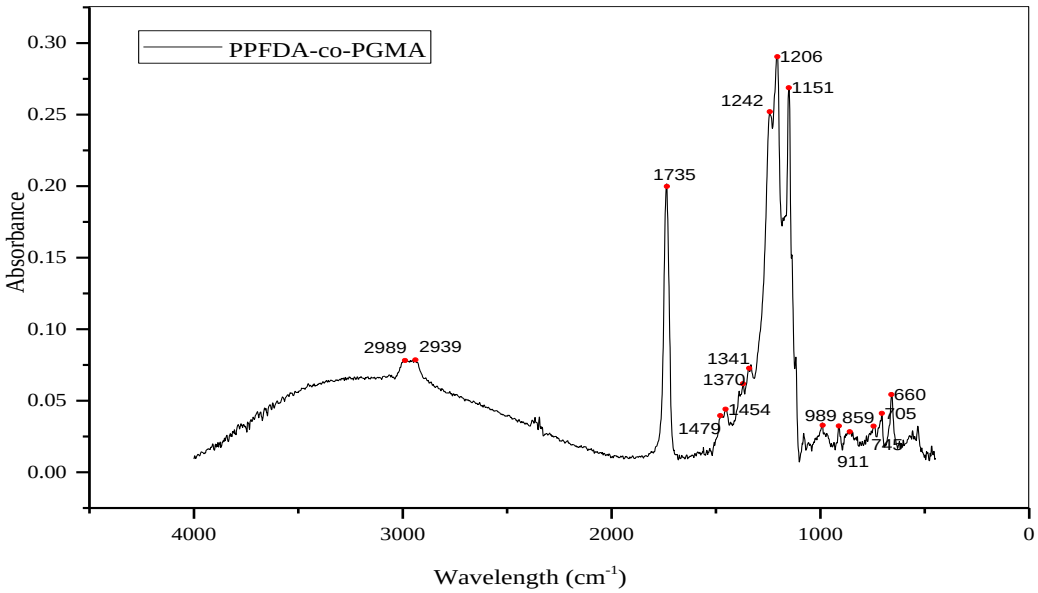

Figure 3.17. FTIR spectra of ~1000 nm thick P(GMA-PFDA) thin film on c-Si

In Figure 3.17, the sharp peak at 1735 cm^{-1} was C=O stretching bond. At the same time, the FTIR spectrum included three strong, sharp absorbance peaks in the 1350-1120 cm^{-1} region. The asymmetric stretching and symmetric stretching of the -CF2- moiety caused the sharp peaks 1206 cm^{-1}, respectively. The -CF2-CF3 end group sharp peak was observed at 1151 cm^{-1}. Furthermore, the characteristic absorbance bands observed at 1479, 1454, 1370 and 989 cm^{-1} are assigned to C=C double bond because of monomers (PFDA and GMA) (Gupta & Gleason et al., 2006). Moreover, these C–H symmetry and asymmetry stretching peaks appeared at 2989 and 2939 cm^{-1} for PPFDA-co-PGMA FTIR spectrum. Besides, in this spectra for GMA epoxy group the characteristic absorption bands were obtained at 911, 859 and 745 cm^{-1} (Bakker & Verlaan et al., 2007). However, these epoxy peaks were less evident than the other FTIR spectra of ~656 copolymer thin film since PFDA composition in copolymer thin film was higher than pure PGMA composition.

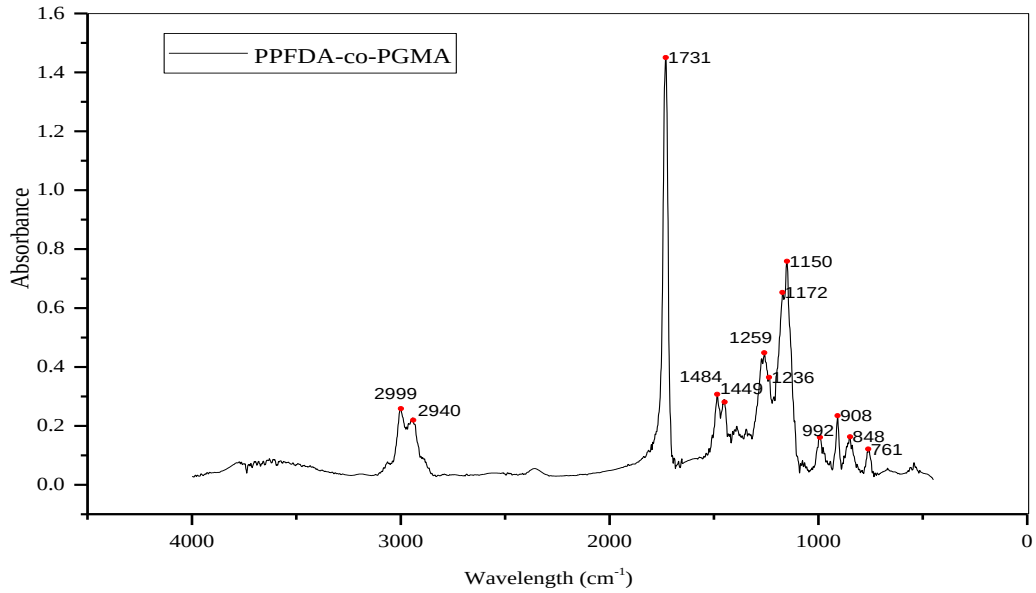

Figure 3.18. FTIR spectra of ~656 nm thick P(GMA-PFDA) thin film on c-Si

C–H symmetry and asymmetry stretching peaks were observed clearly at 2999 and 2940 cm^{-1}. The carbonyl (C=O) stretching vibration due to the ester group the absorption peak was seen at 1731 cm^{-1}. The asymmetric stretching and symmetric stretching of the -CF2- moiety peaks was not observed clearly. However, at 1150 cm^{-1} peak was caused by the -CF2-CF3 end group. The peaks at 1484 and 1449 cm^{-1} existed on the spectrum because of monomer (PFDA and GMA) which were the characteristic absorbance bands for the C=C double bond. At the same time, At 1259, 1236, and 1172 cm^{-1} the three strong peaks were emerged because of GMA structure. Moreover, in the FTIR spectra the characteristic absorption bands were obtained at 908, 848 and 761 cm^{-1} for epoxide groups of GMA (Bakker & Verlaan et al., 2007). The epoxide peaks were obtained clearly, however, the peaks which were belong to PPFDA were not distinct. As a result, the amount of PGMA in its composition was higher than the amount of PPFDA in copolymer film. These findings are also in agreement with deposition conditions where the flow rates of monomers were varied to change the final film composition. However, to determine the composition of materials FTIR analysis is not sufficient, so Nuclear Magnetic Resonance (NMR) spectroscopy should be used in future studies.

3.4. AFM Analysis of Thin Films

Surface morphology and the average surface roughness of deposited polymer films as well as bare glass and c-Si substrates were evaluated by AFM analysis in tapping mode.

3.4.1. AFM Analysis of PGMA Thin Films

For PGMA thin films on c-Si substrates, arithmetic mean roughness (Sa) and root mean square roughness (Sq) values were determined. For this characterization, the uncoated c-Si, 1430 nm PGMA thin film and 367 nm PGMA thin film coated were investigated.

The surface morphology and the surface roughness of uncoated c-Si and PGMA thin films coated on c-Si were examined by scanning 10 μm area and these results were shown in the figures below.

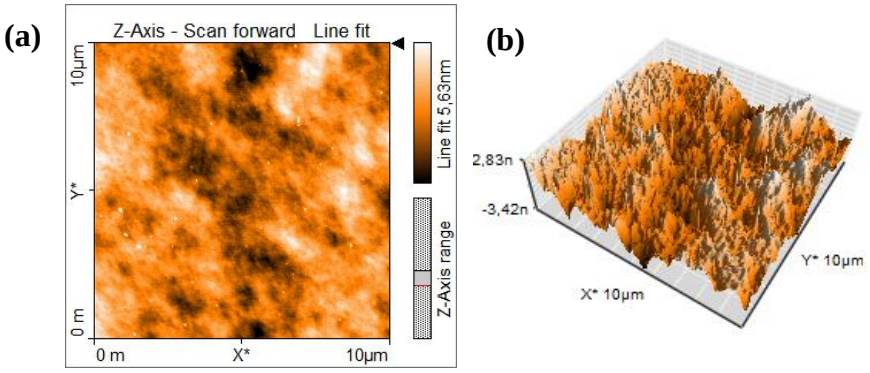

Figure 3.19. AFM results of uncoated c-Si substrate (a) color map (b) 3D view

Figure 3.19 showed that the surface of c-Si was smooth because Sa and Sq values were found as 8.052 and 9.971 Å (angstroms), respectively, indicating a very smooth surface since c-Si substrates were polished beforehand.

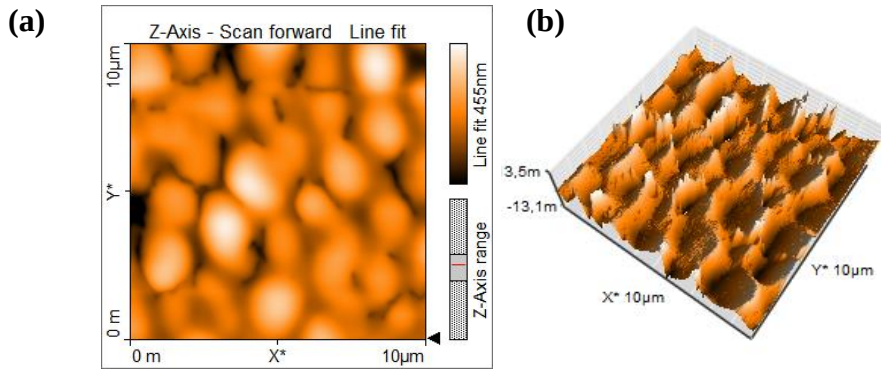

Figure 3.20. AFM results of 1430 nm PGMA thin film on c-Si (a) color map (b) 3D view

The arithmetic mean roughness (Sa) and root mean square roughness (Sq) values of 1430 nm PGMA thin film were obtained as 531.84 Å and 706.28 Å, respectively. As expected, surface roughness of PGMA thin film on c-Si were much higher than the roughness of uncoated c-Si.

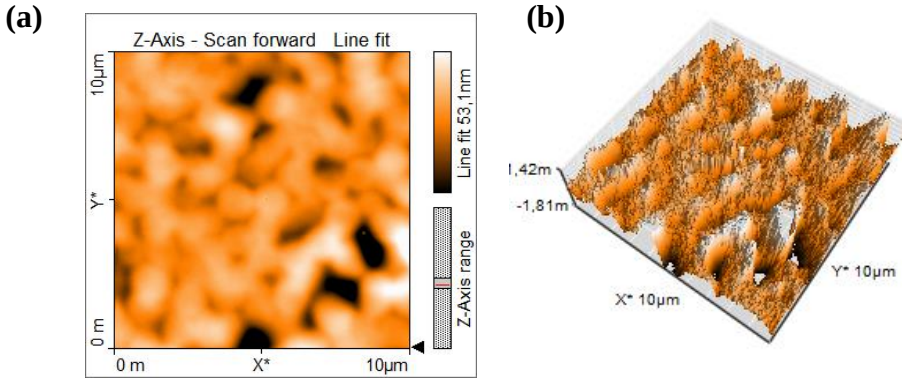

Figure 3.21. AFM results of 367 nm PGMA thin film on c-Si (a) color map (b) 3D view

As seen on Figure 3.21, Sa and Sq values of 367 nm PGMA thin film were calculated as 69.67 Å and 100.24 Å, respectively. Also in literature, the surface roughness was reported to increase with increasing PGMA thin film thickness (Bakker & Verlaan et al., 2007).

3.4.2. AFM Analysis of PCHMA Thin Films

AFM analysis was implemented for surface roughness and morphology of the 975±25 thickness of PCHMA thin film. The result of AFM was given in figure below.

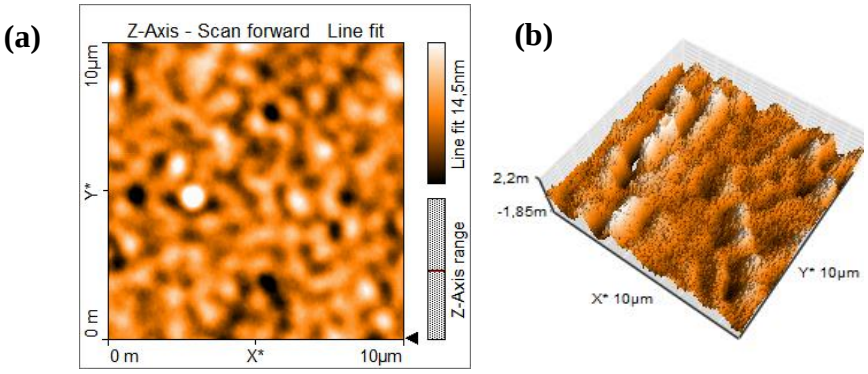

Figure 3.22. AFM results of 975 nm PCHMA thin film on c-Si (a) color map (b) 3D view

According to Figure 3.22, Sa and Sq values were calculated as 19.878 Å and 25.924 Å, respectively. These results showed that the surface roughness was quite low because when the comparison between PCHMA coated c-Si and uncoated c-Si, the surface roughness of samples were close to each other. The surface of PCHMA thin film was smooth like the surface of the uncoated c-Si indicating a very high conformality.

3.4.3. AFM Analysis of PPFDA Thin Films

The result of AFM analysis of 390 nm PPFDA thin film is given in figure below.

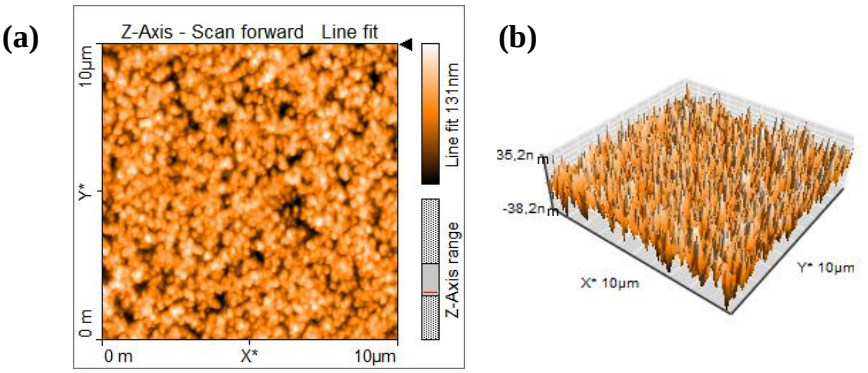

Figure 3.23. AFM results of 390 nm PPFDA thin film on c-Si (a) color map (b) 3D view

As seen on Figure 3.23, the surface of PPFDA thin film was not really smooth. Sa and Sq values were calculated as 176.8 Å and 221.5 Å, respectively. These results showed that the surface roughness of PPFDA thin film on c-Si was higher than the surface roughness of the uncoated c-Si. Besides, compact spherical clusters were present on the surface.

3.4.4. AFM Analysis of P(GMA-PFDA) Thin Films

The results of AFM its surface morphology and roughness of ~1000 nm P(GMA-PFDA) thin film were demonstrated in figures below.

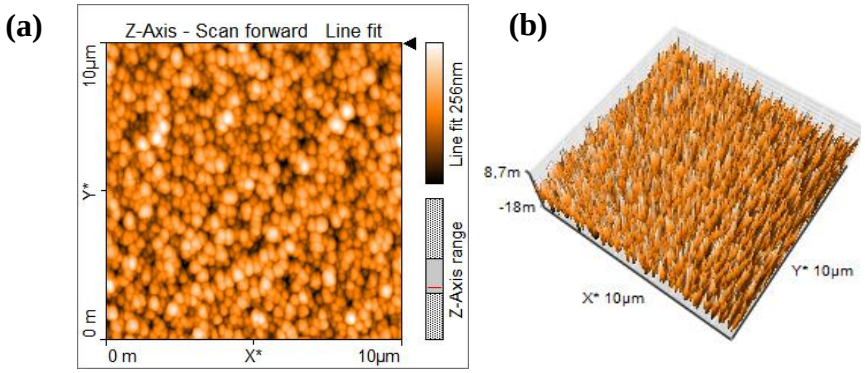

Figure 3.24. AFM results of 1000 nm thick P(GMA-PFDA) thin film on c-Si (a) color map (b) 3D view

In Figure 3.24, the surface morphology of copolymer thin film was observed to be rougher than bare c-Si surface. Sa and Sq values were calculated as 335.16 Å and 417.16 Å, respectively. AFM analysis also revealed that the surface of c-Si was coated with P(GMA-PFDA) thin film. Moreover, 656 nm thick P(GMA-PFDA) thin film was analyzed with AFM. The surface morphology of this copolymer thin film is illustrated in figures below.

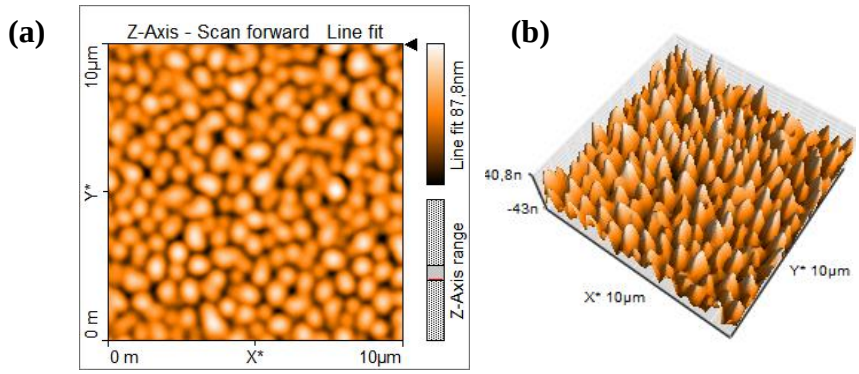

Figure 3.25. AFM results of 656 nm thick P(GMA-PFDA) thin film on c-Si (a) color map (b) 3D view

Figure 3.25 indicated that the surface of copolymer thin film was smoother than previously copolymer thin film because Sa and Sq values were calculated as 122.69 Å and 151.33 Å, respectively. When film thickness was increased, the surface roughness also increased. Therefore, the surface roughness of 656 nm thickness copolymer thin film was lower than the surface roughness of 1000 nm thickness copolymer thin film, as expected.

3.5. Contact Angle Measurement of Thin Films

Perfluoropolymers have low surface tension and wettability. To evaluate the hydrophobicity of perfluoropolymers, contact angle measurement was performed. Water droplet was dropped off from 'I'- shaped needle to the surface of the substrate. Volume of water droplet was adjusted as 6 µL. Drop shape was recorded with a high speed camera attached to the system, and images were then processed by a computer software. The drop shape was evaluated in terms of contact angle automatically as represented by the angle between the substrate surface and a tangent from the edge to the contour of the drop. The contact angle of the water droplet on c-Si was measured on the right and left side. Contact angle measurements of bare c-Si and PPFDA thin film coated c-Si were compared in following figures.

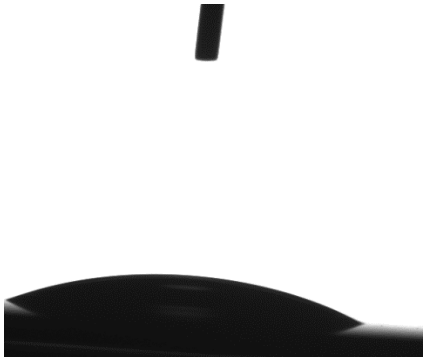

Figure 3.26. The contact angle measurement of the uncoated c-Si

In Figure 3.26, the contact angle was measured as 28.025˚ and 27.506˚ from left side and right side, respectively. Generally, small contact angles (< 90˚) correspond to high wettability. Here, a small contact angle was observed and the water droplet extended on the surface, so the wetting of surface was favorable, indicating a hydrophilic surface.

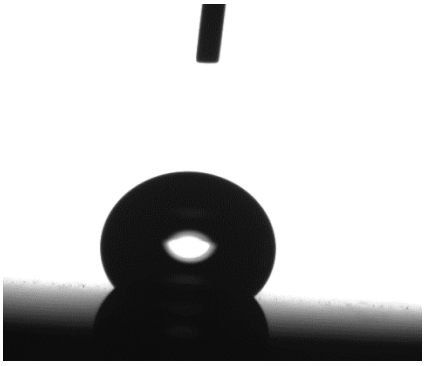

Figure 3.27. The contact angle measurement of the PPFDA thin film coated on c-Si

However, in Figure 3.27, the contact angle was measured as 130.06˚ and 129.78˚ from left side and right side, respectively. The large contact angles (>90˚) correspond to low wettability, so the liquid forms as beads on the surface. It means that the wetting of the surface was unfavorable, therefore the water droplet minimized its contact with the surface and formed a compact water droplet. The hydrophobicity increases with increasing the surface roughness because the roughness provides air entrapment between the surface and the water droplet and also reduces the amount of interaction, so the contact angle increases at hydrophobic surfaces. The roughness of the PPFDA thin film coated surface was an effective parameter to obtain hydrophobic surface. Moreover, the difference of hydrophobicity between the uncoated c-Si and PPFDA thin film coated on c-Si were observed from Figure 3.28.

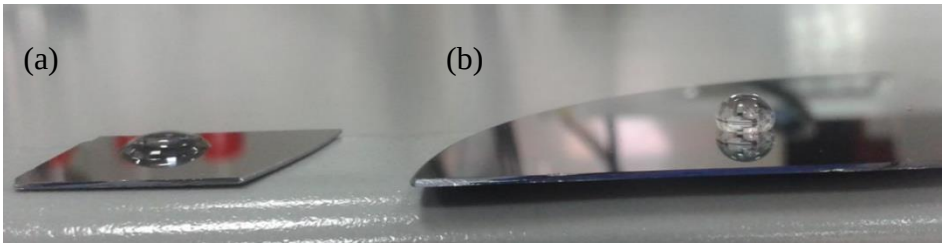

Figure 3.28. (a) The uncoated c-Si and (b) PPFDA thin film coated on c-Si

In addition to c-Si substrate, also paper and tissue paper etc. could be coated with PPFDA. The coated paper, the coated and uncoated tissue paper were demonstrated in following images. A dye and water mixture was dropped on the substrates to reveal surface hydrophobicity.

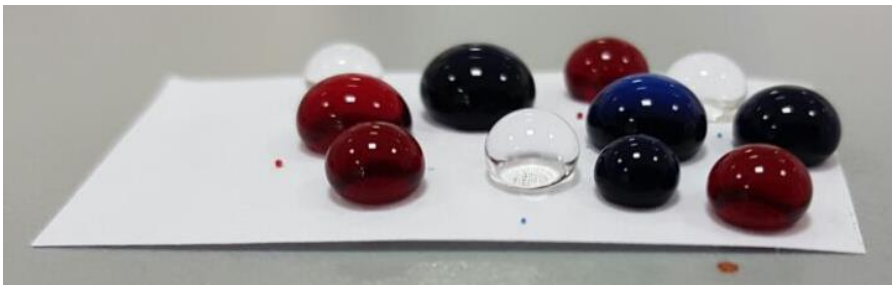

Figure 3.29. PPFDA thin film coated paper

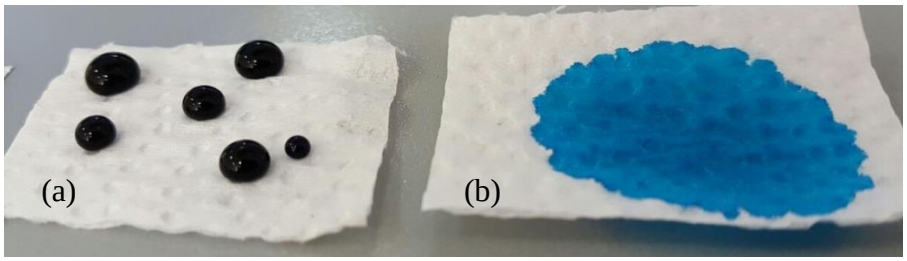

Figure 3.30. (a) PPFDA thin film coated tissue paper and (b) the uncoated tissue paper

According to above Figure 3.29 and Figure 3.30, the super hydrophobic surfaces were obtained with PPFDA coating. The wetting of PPFDA coated surface was unfavorable, however, the dyed water wetted the uncoated tissue paper.. To indicate super hydrophobicity property of PPFDA coated tissue paper, the contact angle measurement was carried out.

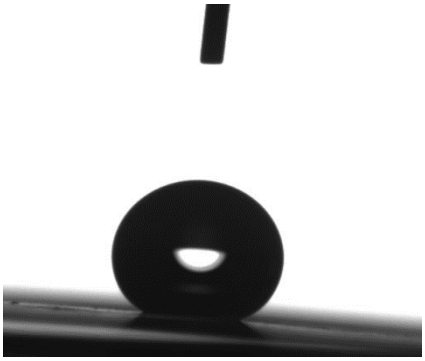

Figure 3.31. The contact angle measurement of the PPFDA thin film coated tissue paper.

Figure 3.31 demonstrated that the contact angle was measured as 150.15˚ and 151.84˚ from left side and right side, respectively. It means that the PPFDA coated tissue paper had large contact angles (>90˚), therefore, the water droplet was also located on the surface as a liquid bead. The wettability was a quite low.

Normally, the contact angle was high for fluoropolymer as seen on Figure 3.27. The contact angle of copolymer P(GMA-PFDA) thin film on c-Si substrate was also performed.

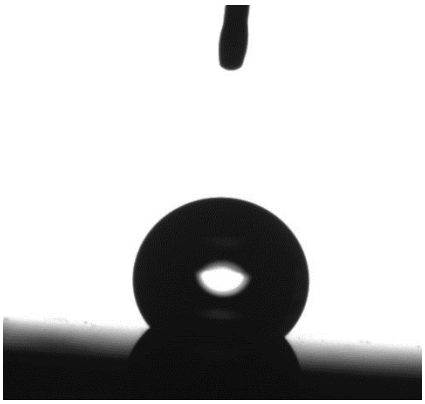

Figure 3. 32. The contact angle measurement of ~ 1000 nm P(GMA-PFDA) thin film on c-Si

In Figure 3.32, the contact angle was measured as 137.06˚ that means, the contact angle was found as desired value because the contact angle was higher than 90˚, so the wettability of surface was low. At the same time, the liquid beads on the surface and the water droplet minimized its contact with the surface. The surface roughness affected on the contact angle. The surface roughness of 1000 nm thickness copolymer thin film enhanced the hydrophobicity of this sample.

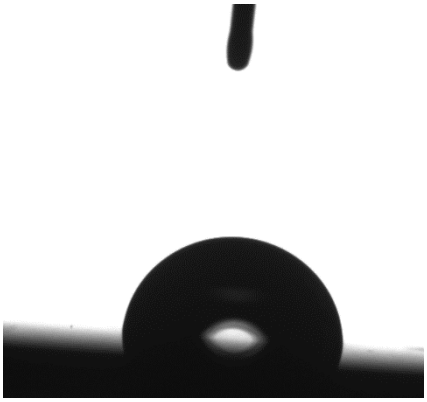

Figure 3.33. The contact angle measurement of 656 nm P(GMA-PFDA) thin film on c-Si

Figure 3.33 illustrated that the average of the contact angle was measured as 87.08˚. This surface provided not too high wettability because the contact angle of surface (87.08˚) was close to critical angle (90˚). The water droplet did not spread on the surface, totally. However, this surface was called as hydrophilic because of small contact angle (< 90˚). The surface roughness which was lower than the previous experiment, so it did not affect the hydrophobicity.

To compare and investigate the effect of PPFDA on copolymer thin film, the contact angle of only PGMA coated thin film on silicon wafer was measured. When the measurement was carried out, the result of 2^{th} experiment (approximately 500 nm) was used. This result was shown in Figure 3.34.

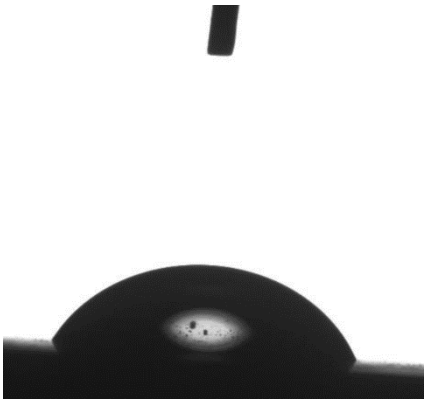

Figure 3.34. The contact angle measurement of ~500 nm PGMA thin film on c-Si

The contact angle of ~500 nm thickness PGMA thin film was found as 65.85°. PGMA thin film surface was hydrophilic because contact angle was smaller than 90°. However, according to the result of 656 nm P(GMA-PFDA) thin film, PPFDA contributed to hydrophobicity because the contact angle increased from 65° to 87.08°.

When the contact angle measurements of copolymer thin films and PGMA thin film were evaluated, the characteristic properties of PPFDA was observed on 1000 nm P(GMA-PFDA) thin film, because the surface was hydrophobic. It was known that the hydrophobicity property was provided with fluoropolymers because of their chemical structure. At the same time, 656 nm P(GMA-PFDA) copolymer thin film on c-Si was not hydrophobic surface because PPFDA amount in copolymer was not enough to contribute hydrophobicity of the surface.

3.6. Performance Tests for Homopolymer and Copolymer Films

To investigate the mechanical properties of both homopolymer and copolymer coating surfaces, some performance tests were performed. After deposition experiments, surface quality of each homopolymer and copolymer film was evaluated by using optical microscopy for scratches, pinholes and other surface defects. Moreover, humidity, swelling in water, salt resistance, solubility in different chemicals, and adhesion tests were carried out (Ozpirin, 2016).

Humidity tests were performed to investigate the coated film resistance to the moisture. For this test, the chamber temperature was 35^{o}C and relative humidity was adjusted as 80-95%. The resistivity of coated thin films to various solvents and water were investigated by applying swelling and solubility in water test. The coated samples were put in beaker which contained deionized water at room temperature for 48 hours. In salt solubility test, a salt solution was prepared with 80 ml water and 3.58 g NaCl. The coated samples were immersed into the salt solution at room temperature for 24 hours. Then, samples were washed with deionized water and dried in oven at 60^{o}C and approximately 30 minutes. Another performance test was the solubility and cleanability test. The homopolymer and copolymer film coatings were immersed into three different solutions which were trichloroethylene, acetone and ethyl alcohol for 20 minutes. In adhesion test, 1.27 cm wide cellophane tape was applied on the surfaces of copolymer films. Homopolymer and copolymer coated film thicknesses were measured by reflectometer before and after the tests mentioned above. The measured thicknesses were almost the same after each test indicating films showed excellent resistance to humidity, salt solubility, and swelling in water and also showed high adhesion to c-Si substrate. Moreover, in adhesion test, it was observed that copolymer with higher amount of GMA

monomer in their structure showed higher adhesion and mechanical strength as expected (Ozpirin, 2016).

CHAPTER 4

CONCLUSIONS

In this study, the fabrication of polymeric protective nano-coatings were carried out on flat, and 3D surfaces via iCVD system. For polymeric protective nano-coatings against dust, humidity and the temperature changes etc. three different monomers were investigated using different deposition parameters to obtain functional surfaces.

iCVD process was selected to obtain protective polymeric thin film among all other coating processes because in iCVD process vapor-to-surface reactions were taken place and, complex and conformal coatings were observed. Besides, in iCVD process the thickness of coating materials over the substrate were controlled well. The polymeric nano-coating was produced as a result of the polymerization reaction in iCVD process. While a variety of polymers were produced, functional organic CVD polymers were used to be gained specific features on the surfaces. In order to obtain coatings with unique properties specified by the application GMA, CHMA and PFDA were used as monomers; GMA for excellent mechanical and adhesion properties and PFDA for providing super hydrophobicity. Homopolymers of PGMA, PCHMA and PPFDA thins films with varying thicknesses were deposited on c-Si and glass substrates via iCVD process. As a result of characterization methods, PGMA thin films showed excellent mechanical and optical properties, but hydrophobicity of the surface was not sufficient to be used as protective coatings. However, PPFDA thin films indicated excellent surface hydrophobicity but also showed very poor mechanical properties. PPFDA thin films were damaged by mechanical handling. In order to obtain polymeric protective thin films which have both of good mechanical properties and hydrophobicity, P(GMA-PFDA) copolymer thin films were fabricated via iCVD process. It was obtained that optical and mechanical properties of copolymers can be controlled with the flow rates of monomers during iCVD deposition process. When the results of experiments were investigated with characterization methods, in FTIR results of the copolymer thin films, the characteristic peaks of PGMA and PPFDA were also observed separately. Moreover, the results of contact angle measurements of copolymer thin films showed that they became super water-repellent surfaces that was known as super hydrophobic surfaces.

iCVD process is suitable to coat the surface of the delicate structure because iCVD process is independent of the substrate temperature. In this way, fibers, cotton textile fabrics can be modified with PPFDA film successfully. Moreover, in chemical processes solvent usages are required to give super hydrophobic properties to shoes and textile materials intensively used in daily life. The solvent usage increases cost and damages the environment, so iCVD process overcome these problems and PPFDA films on industrial scales can be coated at very low costs and without damaging to environment.

Most of the obtained polymeric thin films via iCVD process are acrylic compounds which contain functional groups. Therefore, the selection of monomers containing acrylic compounds is an important to bring new features on surfaces. Considering the purpose of this study and performance tests, to protect the optical surfaces that are especially used in Electro-Optical (EO) systems from external factors (humidity, sudden temperature changes, and dust etc.) because EO systems, which have high maintenance and manufacturing costs, should be protected against all corrosives.

REFERENCES

Aegerter, M. A., & Mennig, M. (2004). Sol-Gel Technologies for Glass Producers and Users: Springer US.

Al-Dahoudi, N. (2003). Wet chemical deposition of transparent conducting coatings made of redispersable crystalline ITO nanoparticles on glass and polymeric substrates (The Doctor of Engineering Sciences), der Universität des Saarlandes

Allcock, H. R., Lampe, F. W., & Mark, J. E. (2003). Contemporary Polymer Chemistry: Prentice Hall.

Askeland, D., Fulay, P., & Wright, W. (2010). The Science and Engineering of Materials: Cengage Learning.

Babilius, K., Babilius, A., & Jurgutis, L. (2014). Research of Ni-Al-O system catalytic coatings developed for gasification and steam reforming processes. Mechanics, 20(3), 317-326.

Bach, H., & Krause, D. (2003). Thin Films on Glass: Springer Berlin Heidelberg.

Bakker, R., Verlaan, V., van der Werf, C. H. M., Rath, J. K., Gleason, K. K., & Schropp, R. E. I. (2007). Initiated chemical vapour deposition (iCVD) of thermally stable poly-glycidyl methacrylate. Surface and Coatings Technology, 201(22–23), 9422-9425.

Bergauer, D. A. (1993). Deposition Methods. Retrieved October 9, 2015, from http://static.ifp.tuwien.ac.at/homepages/Personen/duenne_schichten/pdf/t_p_ds_chapter2.pdf

Birkner, N., & Wang, Q. (2016). How an FTIR Spectrometer Operates. Retrieved April 13, 2016, from http://chemwiki.ucdavis.edu/Core/Physical_Chemistry/Spectroscopy/Vibrational_Spectroscopy/Infrared_Spectroscopy/How_an_FTIR_Spectrometer_Operates

Bradley, L. C., & Gupta, M. (2012). Encapsulation of Ionic Liquids within Polymer Shells via Vapor Phase Deposition. Langmuir, 28(27), 10276-10280.

Callister, W. D. (2010). Materials science and engineering: Hoboken, N.J.: Wiley; Chichester : John Wiley [distributor], 2010. 8th ed., International student ed.

Çetin, N. E., Korkmaz, Ş., Elmas, S., Ekem, N., Pat, S., Balbağ, M. Z., Özmumcu, M. (2013). The structural, optical and morphological properties of CaF2 thin films by using Thermionic Vacuum Arc (TVA). Materials Letters, 91, 175-178.

Chan, K., & Gleason, K. K. (2005). Photoinitiated Chemical Vapor Deposition of Polymeric Thin Films Using a Volatile Photoinitiator. Langmuir, 21(25), 11773-11779.

Chan, K., & Gleason, K. K. (2006). A Mechanistic Study of Initiated Chemical Vapor Deposition of Polymers: Analyses of Deposition Rate and Molecular Weight. Macromolecules, 39(11), 3890-3894.

Chen, C.-H., Li, S.-Y., Chiang, A. S. T., Wu, A. T., & Sun, Y. S. (2011). Scratch-resistant zeolite anti-reflective coating on glass for solar applications. Solar Energy Materials and Solar Cells, 95(7), 1694-1700.

Creighton, J., & Ho, P. (2001). Introduction to chemical vapor deposition (CVD).

Diem, M. (2015). Polarization of Light: Salem Press.

Dorval Dion, C. A., & Tavares, J. R. (2013). Photo-initiated chemical vapor deposition as a scalable particle functionalization technology (a practical review). Powder Technology, 239, 484-491.

Engineering, O. (2015). PID & Process Temperature Controllers. Retrieved March 24, 2016, from http://www.omega.com/prodinfo/temperaturecontrollers.html

Friz, M., & Waibel, F. (2003). Coating Materials. In N. Kaiser & H. Pulker (Eds.), Optical Interference Coatings (Vol. 88, pp. 105-130): Springer Berlin Heidelberg.

Griot, M. (2015). Optical Coatings (pp. 17). United States of America.

Grumezescu, V., Holban, A. M., Iordache, F., Socol, G., Mogoşanu, G. D., Grumezescu, A. M., Chifiriuc, M. C. (2014). MAPLE fabricated magnetite@ eugenol and (3-hidroxybutyric acid-co-3-hidroxyvaleric acid)–polyvinyl alcohol microspheres coated surfaces with anti-microbial properties. Applied Surface Science, 306, 16-22.

Gupta, M., & Gleason, K. K. (2006a). Initiated Chemical Vapor Deposition of Poly(1H,1H,2H,2H-perfluorodecyl Acrylate) Thin Films. Langmuir, 22(24), 10047-10052.

Gupta, M., & Gleason, K. K. (2006b). Large-scale initiated chemical vapor deposition of poly(glycidyl methacrylate) thin films. Thin Solid Films, 515(4), 1579-1584.

Heiting, G. (2015). Eyeglass Lens Coatings: Anti-Reflective, Scratch-Resistant, Anti-Fog and UV. Retrieved September 28, 2015, from http://www.allaboutvision.com/lenses/coatings.htm

Heitmann, W. (1970). Vacuum evaporated films of aluminum fluoride. Thin Solid Films, 5(1), 61-67.

Helsch, G., & Frischat, G. H. (2004). Scratch Resistant Coatings. In M. Aegerter & M. Mennig (Eds.), Sol-Gel Technologies for Glass Producers and Users (pp. 217-221): Springer US.

Hunt, D. I. (2015). Spectroscopy. Retrieved October 8, 2015, from http://www.chem.ucalgary.ca/courses/351/Carey5th/Ch13/ch13-1.html

Im, S. G., Bong, K. W., Lee, C.-H., Doyle, P. S., & Gleason, K. K. (2009). A conformal nano-adhesive via initiated chemical vapor deposition for microfluidic devices. Lab on a Chip, 9(3), 411-416.

Johnson, R. W., Hultqvist, A., & Bent, S. F. (2014). A brief review of atomic layer deposition: from fundamentals to applications. Materials Today, 17(5), 236-246.

Jones, B. (2008). Fluoropolymers for Coating Applications JCT CoatingsTech magazine.

Ku, S.-L., & Lee, C.-C. (2010). Optical and structural properties of silicon nitride thin films prepared by ion-assisted deposition. Optical Materials, 32(9), 956-960.

Lau, K. K. S., & Gleason, K. K. (2006a). Initiated Chemical Vapor Deposition (iCVD) of Poly(alkyl acrylates): A Kinetic Model. Macromolecules, 39(10), 3695-3703.

Lau, K. K. S., & Gleason, K. K. (2006b). Initiated Chemical Vapor Deposition (iCVD) of Poly(alkyl acrylates): An Experimental Study. Macromolecules, 39(10), 3688-3694.

Lau, K. K. S., & Gleason, K. K. (2007). Particle functionalization and encapsulation by initiated chemical vapor deposition (iCVD). Surface and Coatings Technology, 201(22–23), 9189-9194.

Lewis, J. A. (2015). What Are Ceramics? Retrieved September 3, 2015, from http://matse1.matse.illinois.edu/ceramics/ware.html

Lewis, J. A. (2015). What are Metals? Retrieved September 2, 2015, from http://matse1.matse.illinois.edu/metals/ware.html

Lewis, J. A. (2015). What are Polymers? Retrieved September 15, 2015, from http://matse1.matse.illinois.edu/home.html

Licari, J. J. (2003). Coating Materials for Electronic Applications: Polymers, Processing, Reliability, Testing: Elsevier Science.

Lvovsky, A. I. (2013). Fresnel Equations. Encyclopedia of Optical Engineering.

MacLeod, H. A., & Macleod, H. A. (2010). Thin-Film Optical Filters, Fourth Edition: CRC Press.

Malandrino, G. (2009). Chemical Vapour Deposition. Precursors, Processes and Applications. Edited by Anthony C. Jones and Michael L. Hitchman. Angewandte Chemie International Edition, 48(41), 7478-7479.

Mao, Y., & Gleason, K. K. (2006). Vapor-Deposited Fluorinated Glycidyl Copolymer Thin Films with Low Surface Energy and Improved Mechanical Properties. Macromolecules, 39(11), 3895-3900.

Mao, Y., & Gleason, K. K. (2004). Hot Filament Chemical Vapor Deposition of Poly(glycidyl methacrylate) Thin Films Using tert-Butyl Peroxide as an Initiator. Langmuir 20(6): 2484-2488.

Martin, T. P., Kooi, S. E., Chang, S. H., Sedransk, K. L., & Gleason, K. K. (2007). Initiated chemical vapor deposition of antimicrobial polymer coatings. Biomaterials, 28(6), 909-915.

Materion. (2015). Silicon Monoxide, SiO.

Matsumura, H. (2007). Catalytic CVD (Cat-CVD). Retrieved October 15, 2015, from http://www.jaist.ac.jp/profiles/info_e.php?profile_id=96

Mattox, D. M. (1973). Fundamentals of ion plating. Journal of Vacuum Science & Technology, 10(1), 47-52.

McInnes, S. J. P., Szili, E. J., Al-Bataineh, S. A., Xu, J., Alf, M. E., Gleason, K. K., Voelcker, N. H. (2012). Combination of iCVD and Porous Silicon for the Development of a Controlled Drug Delivery System. Acs Applied Materials & Interfaces, 4(7), 3566-3574.

McNaught, A., Wilkinson, A. (1996). Homopolymer Vol. 68. (pp. 2287-2300).

Morgan, E. (2015). Polarized Sunglasses. Retrieved October 8, 2015, from http://www.allaboutvision.com/sunglasses/polarized.htm

Ozkan, E., Lee, S.-H., Liu, P., Tracy, C. E., Tepehan, F. Z., Pitts, J. R., & Deb, S. K. (2002). Electrochromic and optical properties of mesoporous tungsten oxide films. Solid State Ionics, 149(1), 139-146.

Ozpirin., M. (2016). Development of Protective Nano Coatings for Electro-Optical Systems

Paxson, A. T., Yagüe, J. L., Gleason, K. K., & Varanasi, K. K. (2014). Chemical Vapor Deposition: Stable Dropwise Condensation for Enhancing Heat Transfer via the Initiated Chemical Vapor Deposition (iCVD) of Grafted Polymer Films (Adv. Mater. 3/2014). Advanced Materials, 26(3), 349-349.

Perales, F., Herrero, J. M., Jaque, D., & de las Heras, C. (2007). Improvement of MgF2 thin coating films for laser applications. Optical Materials, 29(7), 783-787.

Piegari, A., & Flory, F. (2013). Optical Thin Films and Coatings: From Materials to Applications: Elsevier Science.

Piispanen, M., & Hupa, L. (2011). Comparison of self-cleaning properties of three titania coatings on float glass. Applied Surface Science, 258(3), 1126-1131.

Roberts, J. D., & Caserio, M. C. (1977). Basic Principles of Organic Chemistry: Study Guide: W. A. Benjamin.

Roychoudhuri, C. (2008). Fundamentals of photonics.

Schropp, R. E. (2009). Hot Wire Chemical Vapor Deposition: Recent Progress, Present State of the Art and Competitive Opportunities. ECS Transactions, 25(8), 3-14. doi: 10.1149/1.3207570

Schropp, R. E. I. (2015). Industrialization of Hot Wire Chemical Vapor Deposition for thin film applications. Thin Solid Films.

SemiconSoft, I. (2013). The MProbe System. Retrieved March 30, 2016, from http://www.semiconsoft.com/wp/

Şen, M. Principle Characteristics of Polymers. Retrieved September 20, 2015, from http://www.polymer.hacettepe.edu.tr/webim/msen/polymertechnologylesson/PrincipleCharacteristicsofPolymers.pdf

Seshan, K. (2001). Handbook of Thin Film Deposition: Elsevier Science.

Sok Won, K., Manil, K., Inkoo, K., Minwoo, C., & Ji-Wook, R. (2011). Optical Properties of Sputtered Indium Tin Oxide Thin Films. Journal of Korean Physical Society, 59, 3280.

Spee, D. A., Rath, J. K., & Schropp, R. E. I. (2013). Polymer Layers by Initiated CVD for Thin Film Gas Barrier Encapsulation Encapsulation Nanotechnologies (pp. 255-289): John Wiley & Sons, Inc.

Stenzel, O. (2014). Optical Coatings: Material Aspects in Theory and Practice: Springer.

Tracton, A. A. (2006a). Coatings Materials and Surface Coatings: CRC Press.

Tracton, A. A. (2006b). Coatings Technology: Fundamentals, Testing, and Processing Techniques: CRC Press.

TSP, I. (2012). DURAVUE® Abrasion-Resistant Coatings. Retrieved September 28, 2015, from http://www.tspinc.com/anti-scratch-coatings/

web1. Ceramic Properties. Retrieved September 3, 2015, from http://depts.washington.edu/matseed/mse_resources/Webpage/Ceramics/ceramic property.htm

web2. What is the process of Polymerization? Retrieved September 20, 2015, from http://www.innovateus.net/innopedia/what-process-polymerization

web3. (2015). Composite material. Retrieved September 15, 2015, from https://en.wikipedia.org/wiki/Composite_material

web4. Composites. Retrieved September 15, 2015, from http://www.the-warren.org/GCSERevision/systemsandcontrol/composites.html

web5. (2015). Coating. Retrieved September 22, 2015, from https://www.corrosionpedia.com/definition/286/coating-corrosion

web6. (2013). Teflon and Perfluorooctanoic Acid (PFOA). Retrieved September 22, 2015, from http://www.cancer.org/cancer/cancercauses/othercarcinogens/athome/teflon-and-perfluorooctanoic-acid--pfoa

web7. (2015). Non-stick surface. Retrieved September 22, 2015, from https://en.wikipedia.org/wiki/Non-stick_surface

web8. (2015). Plating. Retrieved September 23, 2015, from http://global.britannica.com/technology/plating

web9. (2015). INDUSTRIAL USES OF ELECTROPLATING. Retrieved September 23, 2015, from http://www.sharrettsplating.com/electroplating-benefits.html

web10. (2015). Plating. Retrieved September 23, 2015, from https://en.wikipedia.org/wiki/Plating

web11. (2015). Plating. Retrieved September 28, 2015, from http://www.plinthandchintz.com/glossary/plating/

web12. Anti-Scratch Coatings - Increased robustness for PC, PMMA and PSU. Retrieved September 28, 2015, from http://www.gxc-coatings.com/products/anti-scratch-coatings.html

web13. Anti-Reflection (AR) Coatings. Retrieved September 28, 2015, from http://www.edmundoptics.com/technical-resources-center/optics/anti-reflection-coatings/

web14. (2015). Reflection, Transmission, and Absorption. Retrieved September 29, 2015, from http://light-measurement.com/reflection-absorption/

web15. WHAT IS LIGHT OR ELECTROMAGNETISM? Retrieved September 30, 2015, from http://www.artinaid.com/2013/04/what-is-light-or-electromagnetism/

web16. Snell's Law and the Index of Refraction. Retrieved September 30, 2015, from http://www.colorado.edu/physics/phys1140/phys1140_sp05/Experiments/O3Fall04.pdf

web17. (2015). BARIUM FLUORIDE: BaF2 windows and BaF2 lenses. Russia, Saint-Petersburg: Alkor crystal optics.

web18. (2015). Chemical Vapor Deposition-CVD variants. Retrieved October 15, 2015, from http://www.dowcorning.com/content/etronics/etronicschem/etronics_newcvd_tutorial3.asp

Wilson, A. D. (2012). Surface Coatings—1: Springer Netherlands.

Xu, J., & Gleason, K. K. (2011). Conformal Polymeric Thin Films by Low-Temperature Rapid Initiated Chemical Vapor Deposition (iCVD) Using tert-Butyl Peroxybenzoate as an Initiator. Acs Applied Materials & Interfaces, 3(7), 2410-2416.

APPENDIX A

CALIBRATION GRAPHS

All mass flow controllers were calibrated with the used monomers and initiator. The calibration graphs were obtained as following figures.

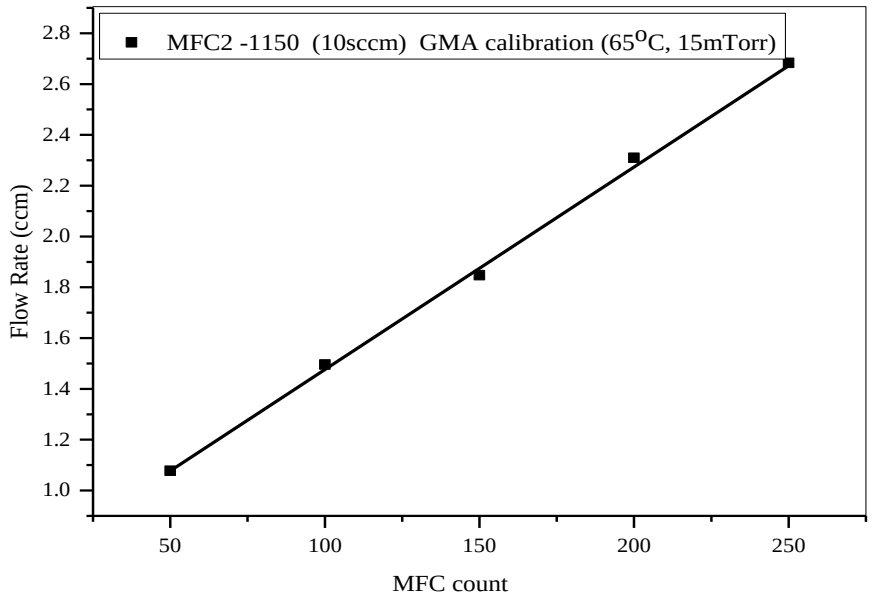

Figure A.1. The calibration graph of GMA

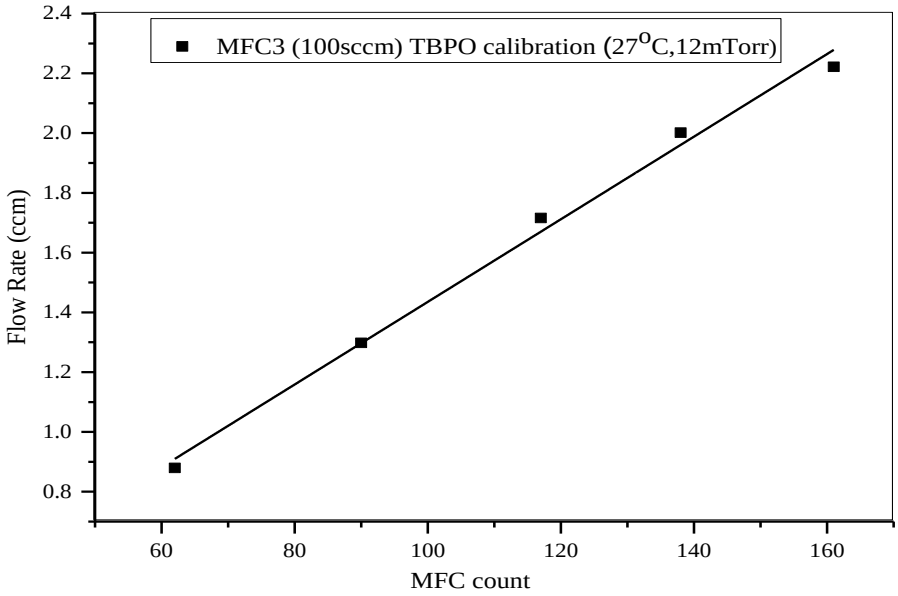

Figure A.2. The calibration graph of TBPO

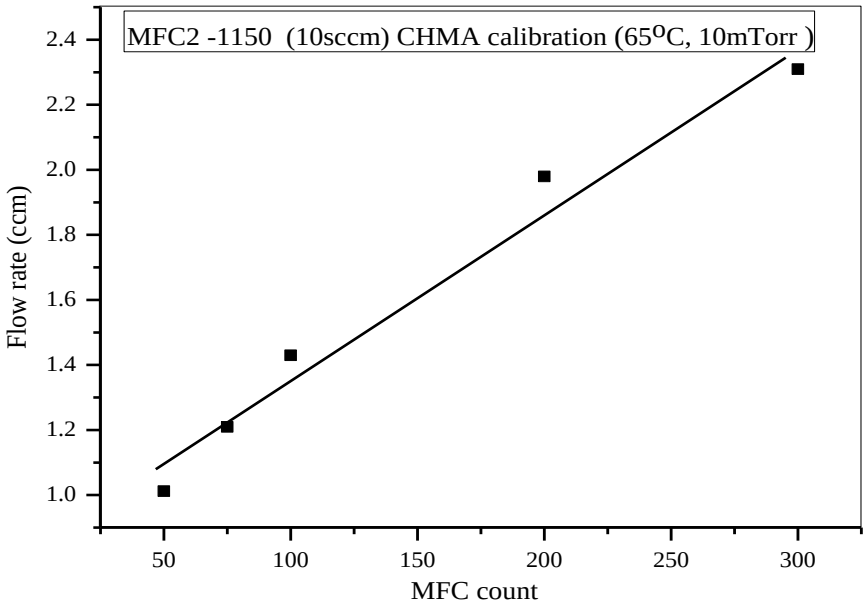

Figure A.3. The calibration graph of CHMA

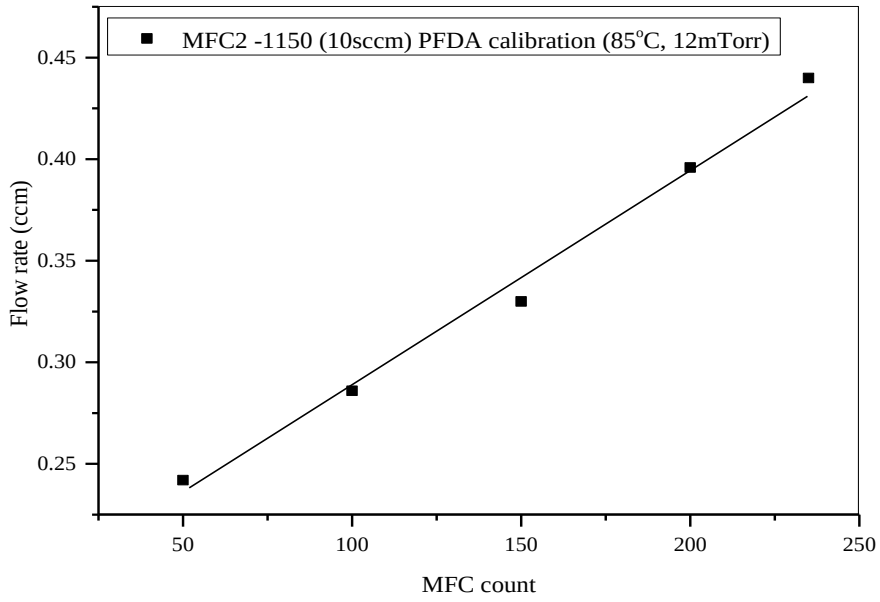

Figure A.4. The calibration graph of PFDA

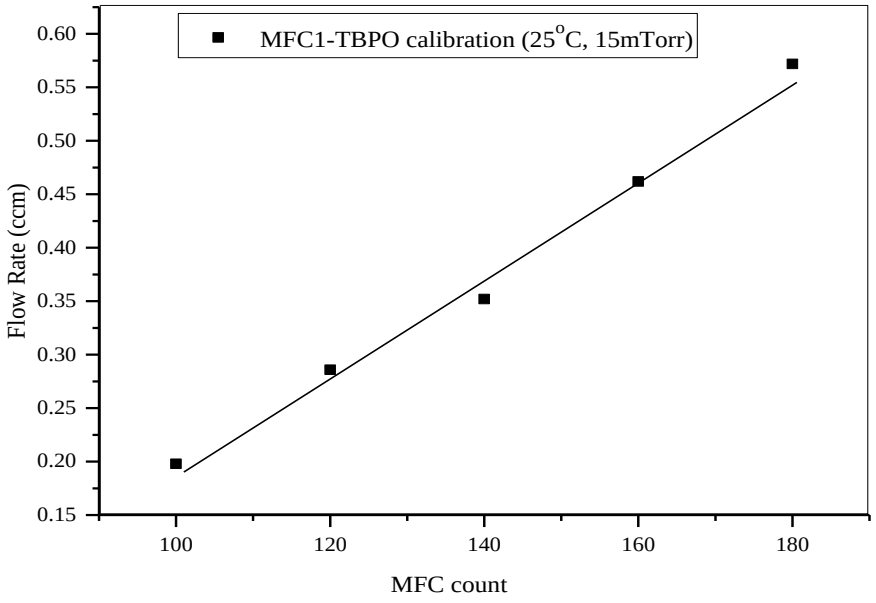

Figure A.5. The calibration graph of TBPO

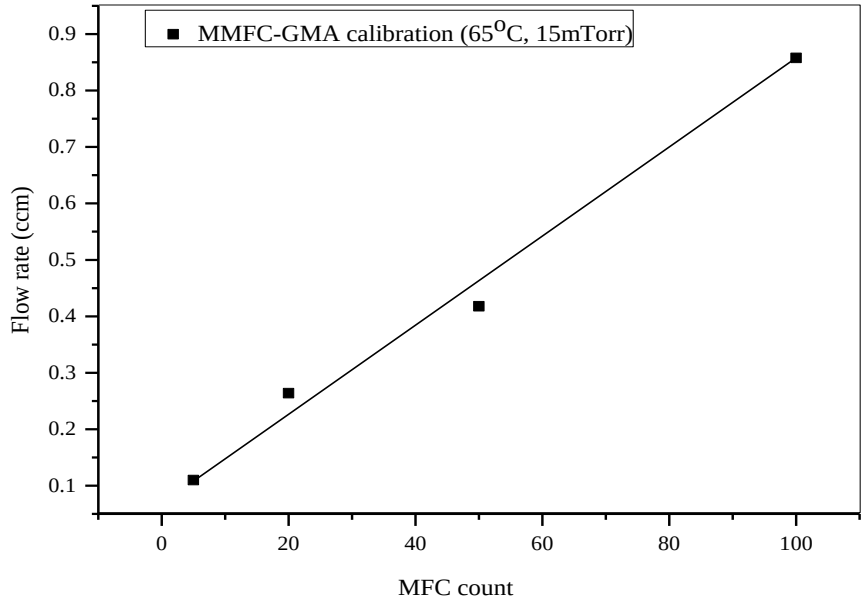

Figure A.6. The calibration graph of GMA